Norm-conserving diffusion Monte Carlo method and diagrammatic expansion of interacting Drude oscillators: Application to solid xenon

Andrew Jones and Andrew Thompson
School of Physics, The University of Edinburgh, Mayfield Road, Edinburgh EH9 3JZ, United Kingdom

Jason Crain
School of Physics, The University of Edinburgh, Mayfield Road, Edinburgh EH9 3JZ, United Kingdom
and National Physical Laboratory, Teddington TW11OLW, United Kingdom

Martin H. Müser
Department of Applied Mathematics, University of Western Ontario, London, Ontario, Canada N6A 5B7

Glenn J. Martyna*
IBM T. J. Watson Research Center, P.O. Box 218, Yorktown Heights, New York 10598, USA
(Received 31 October 2008; revised manuscript received 11 February 2009; published 27 April 2009)

The quantum Drude oscillator (QDO) model, which allows many-body polarization and dispersion to be treated both on an equal footing and beyond the dipole limit, is investigated using two approaches to the linear scaling diffusion Monte Carlo (DMC) technique. The first is a general purpose norm-conserving DMC (NC-DMC) method wherein the number of walkers, N, remains strictly constant thereby avoiding the sudden death or explosive growth of walker populations with an error that vanishes as $\mathcal{O}(N^{-1})$ in the absence of weights. As NC-DMC satisfies detailed balance, a phase space can be defined that permits both an exact trajectory weighting and a fast mean-field trajectory weighting technique to be constructed which can eliminate or reduce the population bias, respectively. The second is a many-body diagrammatic expansion for trial wave functions in systems dominated by strong on-site harmonic coupling and a dense matrix of bilinear coupling constants such as the QDO in the dipole limit; an approximate trial function is introduced to treat two-body interactions outside the dipole limit. Using these approaches, high accuracy is achieved in studies of the fcc-solid phase of the highly polarizable atom, xenon, within the QDO model. It is found that 200 walkers suffice to generate converged results for systems as large as 500 atoms. The quality of QDO predictions compared to experiment and the ability to generate these predictions efficiently demonstrate the feasibility of employing the QDO approach to model long-range forces.

DOI: 10.1103/PhysRevB.79.144119 PACS number(s): 02.70.Ss, 61.50.Lt, 34.20.−b

I. INTRODUCTION

One of the important early applications of quantum mechanics to explain fundamental phenomena was the theoretical demonstration that the interaction between fluctuating dipoles on two rare-gas atoms leads to the experimentally observed temperature-independent attraction which decreases as $1/R^6$ at large separation R (Refs. 1 and 2) and does not arise in the classical limit. This interaction, which is referred to as the pair London force or induced dipole-induced dipole pair dispersion, is usually weaker than other forms of attraction, e.g., those due to permanent charges, dipoles, or quadrupoles, and at short distances, covalent or metallic bonding. Nonetheless, dispersion interactions need to be incorporated realistically if an accurate description of biological, chemical, and physical systems is desired. For instance, if surface tensions are improperly modeled through the neglect of many-body dispersion effects,[3,4] the equilibria associated with the hydrophobic association of biological nanostructures[5] will be shifted.

Incorporating many-body dispersion interactions in both empirical force-field as well as density-functional theory (DFT)-based molecular simulations has proven to be a challenging task. Many-body dispersion interactions in condensed-matter systems are generally modeled by fitting effective pair potential parameters which are optimized to best reflect bulk behavior. However, effective two-body potentials are flawed near surfaces and interfaces leading to errors in the predictions of hydrophobic effects as described above. The leading-order many-body dispersion interaction term is the three-body triple dipole Axilrod-Teller-Muto potential[6] which is not taken into account in standard biophysical force fields.[7] Approximate functionals for DFT that include dispersion are currently being developed but at present are computationally intensive[8] and cannot be applied to large systems.

It has long been suggested that the quantum Drude oscillator model (QDO) (Ref. 2) be employed to generate a high-accuracy force field that can, in turn, be used to drive molecular simulations. The QDO is simply a model atom wherein a single pseudoelectron is bound harmonically to a single pseudonucleus. The QDO thereby naturally treats both many-body dispersion and many-body polarization beyond the dipole limit where the polarization response arises in systems possessing permanent electrostatic moments, and hence a force field based on the QDO would contain intrinsically all long-range interactions. Although the QDO is limited to Gaussian response by construction, given the proper choice

of free parameters, i.e., the charge q, mass m, and the stiffness k of the spring binding a pseudoelectron to its pseudonucleus, it is, for example, possible to accurately reproduce the dipole polarizability given by q^2/k and the induced dipole-induced dipole pair dispersion interaction which additionally depends upon the q/m ratio. More generally, the three parameters q, k, or m can be selected to approximately yield a variety of responses (beyond the dipole limit) via a least-squares fit to values determined either from experiment or high-level electronic structure theory. Other model parameters, such as short-range cutoff functions and short-range repulsive terms, must be fit using more involved procedures.

Recently, it has been demonstrated that QDOs can be applied to study realistic condensed phase systems using a new path-integral molecular dynamics (PIMD) technique[9,10] which in principle gives an exact treatment of the QDO such that the pseudonuclei move at finite temperature on the ground-state Born-Oppenheimer surface provided by the pseudoelectrons of the QDOs. However, PIMD calculations of QDOs are computationally demanding because the large energy-scale separation between the on-site or vacuum energy and the interpseudoatomic coupling terms as well as the need to approach the ground state of the pseudoelectronic degrees of freedom requires the use of large Trotter numbers. Although work by the current authors is in progress to improve the efficiency of the PIMD treatment of QDOs, it is nonetheless useful to pursue alternative approaches such as diffusion Monte Carlo (DMC) capable of generating high-accuracy single-point (fixed atomic configuration) ground-state energies useful in fully specifying the model (e.g., parametrizing short-range repulsions and cutoff functions) through, for example, fits to the results of single-point high-level all-electron computations of small systems.

The DMC method is commonly employed to generate single-point ground-state energies accurately and efficiently. However, the method depends on knowledge of a good approximation to the many-body ground-state wave function. As the pseudoelectrons of QDOs are distinguishable particles, there is no need to antisymmetrize the wave function which simplifies the problem. For distinguishable particles, the wave function can be written as a product of an approximate single-particle trial wave function and a correction factor. In the frequently employed Jastrow trial wave functions,[11] the correction factor takes the functional form $\exp[-\upsilon V]$, where υ is a variational parameter and V is a potential energy. While Jastrow trial wave functions are simple to implement and tend to increase trial function accuracy substantially, they suffer from two disadvantages. First, the term υ needs to be determined numerically via a variational Monte Carlo simulation, and second, a well-defined procedure to systematically improve the wave function beyond two-body interactions is not generally available. For the QDO in the dipole limit, we demonstrate that it is possible to overcome these shortcomings. Using diagrammatic techniques, analytical expressions for $\tilde{V}$ replacing the term υV in the Jastrow trial function can be derived, which include pair dispersion, three-body dispersion, etc. at each successive higher-order diagram. This is accomplished by increasing the complexity of $\tilde{V}$ from a pair potential to a three-body potential, and so on (e.g., $\tilde{V}=\tilde{V}^{(2)}+\tilde{V}^{(3)}+\ldots$) at each order. In addition, we derive an alternative analytical expression for $\tilde{V}^{(2)}$ which includes approximately all pair-wise induced moment–induced moment interactions.

We, also, present a DMC method which enforces norm conservation at every step without modulating the acceptance rule in time or introducing weights building on Refs. 12–14. Our norm-conserving DMC (NC-DMC) technique is developed by considering the evolution of a fixed ensemble of walkers and ensuring that the flux of walkers in and out of the ensemble exactly matches for every instantaneous walker configuration, a property that must be true as the number of walkers in the ensemble goes to infinity. The NC-DMC method is thus formally valid in the large walker limit, satisfies detailed balance, is by construction stable to fluctuations, and statistical averages can be converged to high accuracy. The $\mathcal{O}(N^{-1})$ population bias can be removed by weighting the trajectory both within mean field to lower the magnitude of the $\mathcal{O}(N^{-1})$ error with no overhead and, exactly, in principle, with extra computational overhead. The error to be projected out by the weighting technique vanishes as $\mathcal{O}(N^{-1})$ thereby enhancing the stability of weighting procedure which can be unstable without such improvements.[12]

Finally, QDOs challenge the decomposition of the DMC propagator, limiting the imaginary-time step that can be employed to evolve the ensemble in time. A propagator, exact for Gaussian trial functions but generally applicable, is therefore derived and presented. The NC-DMC method both with and without the new propagator is tested on simple model systems to demonstrate the ability of the technique to convergence to the correct results in practice.

In order to demonstrate the feasibility of using the diagrammatic QDO trial function in conjunction with NC-DMC method to generate high-accuracy single-point energies for the development of high-accuracy force fields, we study the face-centered cubic (fcc) xenon crystal at $T=0$. In the dipole limit of the QDO model, comparisons are made to exact results for the energy as a function of system size. The full QDO model is then examined and the bulk modulus and total energy are computed and compared to experiment.

II. METHODS

Here, the NC-DMC method is presented, first, followed by a discussion of trial functions for the QDO model.

A. Norm-conserving diffusion Monte Carlo (NC-DMC)

DMC permits exact ground-state energies of many-body quantum-mechanical systems to be computed as first proposed by Fermi.[15–20] DMC simulates the evolution of the partial differential equation

$$\frac{\partial \phi}{\partial \beta} = -(\hat{H} - \bar{E})\phi,$$

$$\phi(\beta) = \exp[-\beta(\hat{H} - \bar{E})]\phi(0) = \sum_k \exp[-\beta(E_k - \bar{E})]c_k\psi_k, \tag{1}$$

where $\hat{H}\psi_k = E_k\psi_k$ and $\phi(0) = \Sigma_k c_k\psi_k$. In the large β regime, $\beta(E_1 - E_0) \gg 1$, the asymptotic solution, $\phi \propto \psi_0$, emerges (i.e.,

provided $c_0 \neq 0$) and with the choice $\bar{E}=E_0$ the evolution conserves the "norm," $\int d^3r\phi(\mathbf{r},\beta+\tau)\equiv\int d^3r\phi(\mathbf{r},\beta)$. For bosons and distinguishable particles ψ_0 is nodeless. Thus, DMC possesses a stationary large $\hbar\beta$ or long "imaginary-time" solution. Here we have written the norm conservation equation for a single particle in three-dimensional space for the sake of clarity. The formalism is identical for other particle numbers and dimensions.

In practice, the Hermitian operator $\hat{H}$ is decomposed into a sum of Hermitian operators $\hat{H}=\Sigma_{i=1}^{n_s}\hat{h}_i$, and a Hermitian, approximate evolution operator is constructed. Using $n_s=2$ yields

$$\phi(\beta)=\left[\prod_{k=1}^{P} e^{-\frac{\tau}{2}\hat{h}_1}e^{-\tau\hat{h}_2}e^{-\frac{\tau}{2}\hat{h}_1}\right]\phi(0)$$

$$=\exp[-\beta(\hat{\tilde{H}}(\tau)-E_0)]\phi(0)$$

$$=\sum_k \exp[-\beta(\tilde{E}_k(\tau)-\bar{E})]c_k\psi_k, \qquad (2)$$

where $\hbar\tau=\hbar\beta/P$ is the imaginary-time step and $\hat{\tilde{H}}(\tau)=\hat{H}+\mathcal{O}(\tau^2)$ is a Hermitian operator with ground-state eigenvalue $\tilde{E}_0(\tau)=E_0+\mathcal{O}(\tau^2)$ and eigenstate $\tilde{\psi}_0(\tau)=\psi_0+\mathcal{O}(\tau^2)$ as is easily proved using the Baker-Campbell-Haussdorf formula.[21] With the choice $\bar{E}=\tilde{E}_0(\tau)$, the approximate evolution is norm conserving in the asymptotic regime. However, an appropriately small $\hbar\tau$ must be selected and/or extrapolations to the $\hbar\tau\rightarrow 0$ limit made to generate the desired result. For the usual case, $\hat{H}=\hat{T}+\hat{V}-\bar{E}$, we take $\hat{h}_1=T$ and $\hat{h}_2=\hat{V}-\bar{E}$ to simplify the further development given below.

In order to simulate Eq. (2) to its steady state, an initial wave function is represented by an ensemble of N "walkers," each occurring with probability $\phi(\mathbf{r};0)d\mathbf{r}$ as we restrict the discussion to bosons and distinguishable particles.[16–20] Consider the typical case $\hat{H}=\hat{T}+\hat{V}-\bar{E}$. The evolution of the ensemble by the exponential on the kinetic operator is analogous to the time evolution of a diffusion equation with diffusion coefficient, $D=\hbar/2m$. The normalized potential operator $V-\bar{E}$ is analogous to a differential survival operator in biology: increasing or decreasing the local density according to the local potential while conserving the norm of the total density. The diffusion, branching/annihilation, diffusion, time evolution or "diffusion" Monte Carlo random walk generates a distribution of walkers representative of the ground-state wave function in the long imaginary-time limit as demonstrated above in the imaginary-time step, $\hbar\tau$, approaches zero limit. For systems consisting of identical particles (unlike the QDO), the Bose-ground state is generated and ψ_0 is nodeless unless special measures are taken to project this solution out.[16–20] For systems with hard walls (e.g., $V\rightarrow\infty$ in a region of space as opposed to a point of measure zero), it is possible to derive more complex approximations to propagators[16–20] for which the diffusion move satisfies the boundary conditions. Lacking improved propagators, very slow convergence with $\hbar\tau$ is observed. (When employing propagators that generate boundary-condition violations, it is useful to take $\hat{h}_2=T$ and $\hat{h}_1=\hat{V}-\bar{E}$.) Singularities associated with undamped attractive Coulomb potentials can also be overcome with improved propagators.

Although it is possible to simulate Eq. (1) and achieve well-converged ground-state energies, it is more efficient to introduce a trial wave function ψ_T, which is a good approximation to ψ_0, and write a differential equation for the product $f(\beta)=\psi(\beta)\psi_T$. For the usual case $\hat{H}=\hat{T}+\hat{V}$,

$$\frac{\partial f}{\partial\beta}=-(\hat{T}+\hat{V}_{\text{eff}}+\hat{D})f=-\hat{O}f,$$

$$f(\beta)=\psi_T\sum_k \exp[-\beta(E_k-\bar{E})]c_k\psi_k, \qquad (3)$$

where

$$\hat{V}_{\text{eff}}=\frac{(\hat{H}-\bar{E})\psi_T}{\psi_T},$$

$$\hat{D}f=\frac{\hbar^2}{m}\nabla[f\nabla\ \log\ \psi_T]. \qquad (4)$$

Taking $\bar{E}=E_0$, the distribution $f(\beta)\rightarrow\psi_0\psi_T$ in the large $\hbar\beta$ limit and the evolution conserves the norm $\int d^3rf(\mathbf{r},\beta)\equiv\int d^3rf(\mathbf{r},\beta+\tau)$ which again demonstrates the existence of a stationary long imaginary-time solution. The discussion remains limited to bosons and distinguishable particles (and fixed node fermion simulations). This approach is often referred to as DMC with importance sampling. The more basic approach is recovered by setting $\psi_T=1$.

In the limit that ψ_T is a good approximation to ψ_0, the operator $\hat{V}_{\text{eff}}$ approaches zero thereby improving short imaginary-time approximations to the evolution operator and reducing the number of iterations required to reach the asymptotic regime. However, $\hat{O}$ is not a Hermitian operator complicating the analysis of the approximate evolution. In that, it shall be assumed that any appropriate splitting generates the solution

$$f(\beta)=\tilde{\psi}_T(\tau)\sum_k \exp[-\beta(\tilde{E}_k(\tau)-\bar{E})]c_k\tilde{\psi}_k(\tau) \qquad (5)$$

as above and that selecting $\bar{E}=\tilde{E}_0(\tau)$ leads to a stationary large β solution. The usual choice of splitting is $\hat{O}=\hat{o}_1+\hat{o}_2$, where $\hat{o}_1=\hat{T}+\hat{D}$ and $\hat{o}_2=\hat{V}_{\text{eff}}$. It is easy to show that non-Hermitian evolution operator $\exp(-\tau\hat{o}_1)$, referred to as the drift-diffusion evolution operator, preserves $\exp(-\tau\hat{o}_1)\psi_T^2=\psi_T^2$. However, $\exp(-\tau\hat{o}_1)$ also preserves the norm of an arbitrary f given f and ψ_T are well behaved at the boundaries as can be demonstrated via an integration by parts at each order of τ in a Taylor expansion of the operator acting on f. Given drift-diffusion evolution preserves the norm of the steady-state solution; if the overall approximate evolution is to preserve the norm of the steady-state solution, then the branch evolution must also preserve the norm, i.e., for the ground state, the expected number of "births" per walker, $\langle n^{(+)}\rangle$, should match the expected number of "deaths" per walker, $\langle n^{(-)}\rangle$, as is defined in the following:

$$\int d\mathbf{r}\, \exp[-\tau V_{\mathrm{eff}}(\mathbf{r})]\bar{f}(\mathbf{r}) = \int d\mathbf{r}\bar{f}(\mathbf{r}),$$

$$\int d\mathbf{r}(\exp[-\tau V_{\mathrm{eff}}(\mathbf{r})]-1)\bar{f}(\mathbf{r}) = 0,$$

$$\int d\mathbf{r}\{1-\exp[-\tau V_{\mathrm{eff}}(\mathbf{r})]\}\theta^{(+)}[V_{\mathrm{eff}}(\mathbf{r})]\bar{f}(\mathbf{r})$$

$$= \int d\mathbf{r}\{\exp[-\tau V_{\mathrm{eff}}(\mathbf{r})]-1\}\theta^{(-)}[V_{\mathrm{eff}}(\mathbf{r})]\bar{f}(\mathbf{r}),$$

$$\langle n^{(-)}\rangle_{\bar{f}} = \langle n^{(+)}\rangle_{\bar{f}}. \tag{6}$$

Here, $\bar{f}(\mathbf{r})$ represents the action of $\exp(-\tau\hat{o}_1)$ on the steady-state solution, $f(\mathbf{r})=\tilde{\psi}_T(\mathbf{r};\tau)\tilde{\psi}_0(\mathbf{r};\tau)$, $\theta^{(+)}(x)=1;x\geq 0$ and 0 otherwise, while $\theta^{(-)}(x)=1;x<0$ and 0 otherwise. The desired condition simply states that the flux into $\exp(-\tau\hat{o}_2)\bar{f}$, $\langle n^{(+)}\rangle_{\bar{f}}$, must be balanced by the flux out of $\exp(-\tau\hat{o}_2)\bar{f}$, $\langle n^{(-)}\rangle_{\bar{f}}$. Given that the flux-matching condition needs only hold for the steady-state solution, it is clear that a unique $\bar{E}$ that satisfies Eq. (6) can be found which supports the existence of the assumed Eq. (5) and the corresponding stationary solution.

Some basic considerations are now given. A valid Monte Carlo method need only preserve the stationary solution (assuming ergodic moves). In the Appendix A 1, a discussion of the application of $\exp(-\tau\hat{o}_1)$ for the Gaussian-dominated ψ_T of interest in this paper is given. Finally, the "flux in" is equal to the "flux out" only on average. Therefore, for a finite walker population, the number of walkers in a DMC simulation will fluctuate in time (e.g., unless $\psi_T\equiv\psi_0$).

The foregoing analysis of the stationary solution of the split operator DMC method gives insight into construction of a norm-conserving or constant N, DMC or NC-DMC method. Consider an ensemble of N walkers $(\{\mathbf{r}_1\ldots\mathbf{r}_N\}=\vec{\mathbf{r}})$ (each one for the sake of clarity consisting of a single particle moving in three spatial dimensions) selected with probability $\Pi_i f(\mathbf{r}_i;0)d^3r_i$. Application of the norm-conserving drift-diffusion term to each ensemble member is straightforward and standard as described in Refs. 16–20 and in Appendix A 1 as the N-walker system is separable for this operator. In light of the discussion in the previous paragraph, it is natural to consider the entire ensemble in developing a method to apply the branch evolution, $\exp(-\tau\hat{o}_2)$. As described above, flux matching $\langle n^{(-)}\rangle_{\bar{f}}=\langle n^{(+)}\rangle_{\bar{f}}$ is true on average but not instantaneously $n^{(-)}(\mathbf{r})\neq n^{(+)}(\mathbf{r})$. It is natural to replace the average by a sum over walkers, however, $(1/N)\Sigma_i n^{(+)}(\mathbf{r}_i)\neq(1/N)\Sigma_i n^{(-)}(\mathbf{r}_i)$ unless $N\to\infty$.

It is therefore proposed to enforce norm conservation at each branching step, by enforcing flux balance for the instantaneous N-walker configuration, through a modification to the acceptance rule in the spirit of Refs. 12–14. This is accomplished by defining

$$\bar{n}^{(\pm)}(\vec{\mathbf{r}}) = \frac{1}{N}\sum_i n^{(\pm)}(\mathbf{r}_i),$$

$$w^{(\pm)}(\vec{\mathbf{r}}) = \frac{\bar{n}^{(+)}(\vec{\mathbf{r}})+\bar{n}^{(-)}(\vec{\mathbf{r}})}{2\bar{n}^{(\pm)}(\vec{\mathbf{r}})}, \tag{7}$$

and taking

$$P^{(\pm)}(i;\vec{\mathbf{r}}) = w^{(\pm)}(\vec{\mathbf{r}})n^{(\pm)}(\mathbf{r}_i), \tag{8}$$

where $P^{(\pm)}(i;\vec{\mathbf{r}})d\vec{\mathbf{r}}$ is probability walker and i contributes to the flux into/out of the new ensemble (e.g., the action of the branch operator). The modification creates the "flux-matching branch operator" for each walker

$$\langle\vec{\mathbf{r}}|\exp[-\tau\hat{o}_2]|\vec{\mathbf{r}}\rangle \equiv \{w^{(+)}(\vec{\mathbf{r}})n^{(+)}(\mathbf{r}_i) - \mathrm{Min}[w^{(-)}(\vec{\mathbf{r}})n^{(-)}(\mathbf{r}_i),1]+1\} \tag{9}$$

defined for $N>1$ which when summed over $i=1,N$ yields unity by definition. In more detail, a self-consistent computation is required,

$$w^{(-)}(\vec{\mathbf{r}})\bar{n}^{(-)}(\vec{\mathbf{r}}) = \frac{1}{N}\sum_i \mathrm{Min}[w^{(-)}(\vec{\mathbf{r}})n^{(-)}(\mathbf{r}_i),1],$$

$$w^{(-)}(\vec{\mathbf{r}}) = \frac{w^{(-)}(\vec{\mathbf{r}})\bar{n}^{(-)}(\vec{\mathbf{r}})}{4w^{(-)}(\vec{\mathbf{r}})\bar{n}^{(-)}(\vec{\mathbf{r}})-2\bar{n}^{(+)}(\vec{\mathbf{r}})} > 0, \tag{10}$$

to ensure the ensemble branch operator is positive definite $w^{(-)}(\vec{\mathbf{r}})n^{(-)}(\mathbf{r}_i)\leq 1$; in practice, self-consistent cycles can be avoided as will be discussed in the AppendixA. The selection of the parameter $\bar{E}$ is discussed below. The quantity $w^{(\pm)}(\vec{\mathbf{r}})$ approaches unity as $N\to\infty$ and the branch operator properly reduces to the original form. However, the N-dimensional potential defined by taking the negative logarithm of Eq. (9) has a discontinuous first derivative when a walker's energy changes from $\bar{E}+\delta$ to $\bar{E}-\delta$ because $w^{(-)}(\vec{\mathbf{r}})\neq w^{(+)}(\vec{\mathbf{r}})$ for finite N. This difficulty can be easily overcome by introducing a smooth switching function on a length scale on the order of the standard deviation of $\bar{V}_{\mathrm{eff}}(\vec{\mathbf{r}})=(1/N)\Sigma_i V_{\mathrm{eff}}(\mathbf{r}_i)$ that acts to exclude walkers with energies near $\bar{E}$ from scaling by the weights and vanishes as $1/\sqrt{N}$. At present, this additional improvement has not proved to be necessary. Our approach is not equivalent to that of Ref. 12–14.

The NC-DMC method strictly conserves the number of walkers in the ensemble and hence ensures the stability of the simulation for any reasonable choice of $\bar{E}$. Thus, neither a rare fluctuation far away from flux matching nor a small deviation, $\bar{E}=\tilde{E}_0(\tau)+\delta$, can cause the walker population to grow or shrink by an unacceptably large amount as in the original method. Unlike standard DMC, the NC-DMC acceptance rule does not modulate in time and NC-DMC strictly satisfies detailed balance. Therefore, statistical averages can be converged to high accuracy and the $\mathcal{O}(N^{-1})$ bias can be removed[12–14] as described below. In the Appendix A 2, details of the branching process are given along with prescriptions (i) to check for the correctness of the simulation results, (ii) to treat configurations of measure zero wherein the ensemble branch operator becomes undefined or nearly so (e.g., requiring self-consistent cycles), and (iii) to treat systems

where boundary-condition violations $[n^{(-)}(\mathbf{r}_i) \equiv 1$ for any $i]$ cannot be avoided (whence the above definitions of $\hat{o}_1$ and $\hat{o}_2$ should be reversed).

The NC-DMC method has a bias that leads to $\mathcal{O}(N^{-1})$ error as in standard DMC with its time varying acceptance rule. However, under NC-DMC it is possible to correct for the bias by defining appropriate weights in the usual way. We begin by rewriting the ensemble branch operator

$$\langle \vec{\mathbf{r}}|\exp[-\tau\hat{o}_2]|\vec{\mathbf{r}}\rangle = \exp[-\tau V_{\text{eff}}(\mathbf{r}_i)] \times \exp\{\log\{1+[w^{(+)}(\vec{\mathbf{r}})-1]n^{(+,\dagger)}(\mathbf{r}_i) - [w^{(-)}(\vec{\mathbf{r}})-1]n^{(-,\dagger)}(\mathbf{r}_i)\}\}, \tag{11}$$

where the minimum condition was removed for simplicity and

$$n^{(\pm,\dagger)}(\mathbf{r}_i) = e^{\tau V_{\text{eff}}(\mathbf{r}_i)} n^{(\pm)}(\mathbf{r}_i). \tag{12}$$

The weighting factor for each walker is then

$$W^{(\text{corr})}(\mathbf{r}_i,\vec{\mathbf{r}};\tau) = \exp\{-\log\{1+[w^{(+)}(\vec{\mathbf{r}})-1]n^{(+,\dagger)}(\mathbf{r}_i) - [w^{(-)}(\vec{\mathbf{r}})-1]n^{(-,\dagger)}(\mathbf{r}_i)\}\}. \tag{13}$$

Accumulating the weights for imaginary projection time, $L\hbar\tau$, requires NL extra storage and communication (for parallel computations) and in principle, removes all population biases for sufficiently large L. It is also possible to define a mean-field correction that provides a weight for the entire ensemble and thus introduces extra storage of size L and no additional communication overhead

$$W^{(\text{corr,mf})}(\vec{\mathbf{r}};\tau) = \exp\left\{-\frac{1}{N}\sum_i \log\{1+[w^{(+)}(\vec{\mathbf{r}})-1]n^{(+,\dagger)}(\mathbf{r}_i) - [w^{(-)}(\vec{\mathbf{r}})-1]n^{(-,\dagger)}(\mathbf{r}_i)\}\right\}. \tag{14}$$

The mean-field weight distinguishes "good collections" of size N from "better collections" of size N thereby correcting approximately for the effect of the strict norm constraint.

Under NC-DMC, the parameter, $\bar{E}$, can naturally be determined so the average of the correction in mean field is zero. Assuming the simulation is performed using a good estimate $\bar{E}=\bar{E}_{\text{true}}+\delta$,

$$\bar{E}_{\text{true}} = \bar{E} - \frac{\langle \log[W^{(\text{corr,mf})}(\vec{\mathbf{r}};\tau)]\rangle}{\left\langle \frac{d\log[W^{(\text{corr,mf})}(\vec{\mathbf{r}};\tau)]}{d\bar{E}}\right\rangle} + \mathcal{O}(\delta^2), \tag{15}$$

where the average is not corrected. This result reduces to the standard condition

$$\bar{E}_{\text{true}} = \bar{E} + \frac{\langle \bar{n}^{(-)} - \bar{n}^{(+)}\rangle}{\tau\langle \bar{n}^{(+)} - \bar{n}^{(-)} + 1\rangle} + \mathcal{O}(\delta^2) = \bar{E} + \frac{\langle \bar{n}^{(-)} - \bar{n}^{(+)}\rangle}{\tau} + \mathcal{O}(\delta^2) \tag{16}$$

as $N\to\infty$. The derivatives required in Eq. (15) can be computed simply and efficiently as only parameter differentiation of relatively simple functions is required (e.g., the procedure does not require derivatives of $H\psi_T/\psi_T$ of any kind). Note that computations can be performed with reasonably optimized but imperfect $\bar{E}$ because errors are accounted for by the corrections.

It is well known that statistical averages of exponentiated potential-like terms over nontrivial distributions do not converge if the terms are large. Hence, there is an extensive literature devoted to enhanced sampling techniques such as the weighted histogram method and umbrella sampling which help to overcome these difficulties.[22] This work and that of Refs. 12–14 are in part attempts to approach this general problem as it arises in DMC. Here, as magnitude of error correction scales favorably with walker number, vanishing as N^{-1}, a stable weighting technique results.[12–14] Although in the following, we shall not apply the weighting procedure, the effect of the mean-field correction is examined in the AppendixA. The number of walkers required to obtain a given accuracy is reduced by a factor of ≈ 4 for the model studied.

B. Quantum Drude model

As mentioned in Sec. I, we consider a pseudoelectron with charge $-q$ and mass m pinned via a harmonic spring of stiffness k to its pseudonuclei which is the assigned charge $(Q+q)$, where Q is the permanent charge (here, we take $Q\equiv 0$). Denoting the γ component of the charge's position by r_γ (e.g., $r_1=x, r_2=y, r_3=z$) and that of the pseudonucleus by R_γ, the unperturbed Hamiltonian h_0 becomes

$$h_0 = -\frac{\hbar^2}{2m}\nabla_\gamma^2 + \frac{k}{2}(r_\gamma - R_\gamma)^2, \tag{17}$$

where the summation convention over Cartesian coordinates labeled with Greek indices is implied and where $\nabla_\gamma = \partial/\partial r_\gamma$. Defining $\omega_0=\sqrt{k/m}$, the ground-state eigenenergy of uncoupled system or the "vacuum" energy is

$$E_0 = \frac{3M}{2}\hbar\omega_0, \tag{18}$$

with ground-state wave function

$$\psi_0 = \prod_{i=1}^{M}\phi_{0i},$$

$$\phi_{0i} = \left(\frac{m\omega_0}{\pi\hbar}\right)^{1/4}\exp\left(-\frac{m\omega_0(r_{i\gamma}-R_{i\gamma})^2}{2\hbar}\right), \tag{19}$$

for an M QDO system in three spatial dimensions. For the full Drude oscillator model the intermolecular coupling is simply the Coulomb interaction between all charges in the system (e.g., the intramolecular or on-site interaction is harmonic). The QDO model, thus, has all the long-range responses of a full electronic system, but due to its simple Gaussian response, the QDO cannot describe short-range interactions adequately (e.g., when pseudonuclear separations approach the covalent or van der Waals radius). Hence, suitable cutoff functions are introduced at short distances[9,10] which for clarity will be eliminated from the discussion below.

1. QDO model in the two-body dipole limit

In order to make progress defining approximate trial wave functions, it is useful to change to variables appropriate for the dipole limit.[2] After discussing the dipole limit of the QDO in detail, we shall return to the notation of Eq. (17). Now, introducing the γ component of the instantaneous dipole moment as $\mu_\gamma = q(r_\gamma - R_\gamma)$ and defining $\bar{\nabla}_\gamma = \nabla_\gamma / q$ and $\bar{m} = m/q^2$, the on-site Hamiltonian can be re-expressed as

$$h_{0,i} = -\frac{\hbar^2}{2\bar{m}}\bar{\nabla}_{i\gamma}^2 + \frac{\bar{m}\omega_0^2}{2}\mu_{i\gamma}^2, \tag{20}$$

where $\alpha = q^2/k$ is the dipole polarizability of the QDO model.[2] This change of variables does not alter the form of the vacuum energy but does trivially modify the form of the unperturbed wave function

$$\phi_{0i} = \left(\frac{\bar{m}\omega_0}{\pi\hbar}\right)^{1/4} \exp\left\{-\frac{\bar{m}\omega_0(\mu_{i\gamma} - R_{i\gamma})]^2}{2\hbar}\right\}. \tag{21}$$

In the ideal dipole limit, the interaction v' between the two dipoles can be written as

$$v'_{12} = -\mu_{1\gamma} T_{\gamma\beta}(\mathbf{R}_{12})\mu_{2\beta}, \tag{22}$$

where the vector $\mathbf{R}_{12}$ connects dipoles 1 and 2 and where $T_{\gamma\beta}(\mathbf{R})$ is defined as

$$T_{\gamma\beta}(\mathbf{R}) = \frac{1}{R^5}(3R_\gamma R_\beta - R^2\delta_{\gamma\beta}). \tag{23}$$

Next, we consider two interacting Drude oscillators. The two-body Hamiltonian H_2 can thus be written as

$$H_2 = \sum_{i=1}^{2} h_{0i} + v'_{12} \tag{24}$$

and diagonalized exactly because it is quadratic. This can be achieved with a (unitary) transformation on the variables $\tilde{\mu}^{\pm}$,

$$\tilde{\mu}_\gamma^{\pm} = \frac{1}{\sqrt{2}}(\mu_{1\gamma} \pm \mu_{2\gamma}), \tag{25}$$

which leaves the form of the on-site Hamiltonian $h_{0,i}$ in Eq. (20) invariant, but changes v' to

$$v'_{\pm} = \pm \tilde{\mu}_\gamma^{\pm} T_{\gamma\beta} \tilde{\mu}_\beta^{\pm}. \tag{26}$$

Because we are dealing with point atoms, we can proceed by using an arbitrary director for the vector $\mathbf{R}_{12}$, e.g., by choosing $\mathbf{R}_{12} = (0,0,R)$. As we have now broken the tensor properties of the T-interaction matrix, we denote the x, y, and z components explicitly, i.e., $T_{xx} = T_{yy} = -1/R^3$ and $T_{zz} = 2/R^3$. H_2 is now the sum of two Hamiltonians $\tilde{h}^{\pm}$ each consisting of three independent summands $\tilde{h}_{xx}^{\pm} = \tilde{h}_{yy}^{\pm}$ and $\tilde{h}_{zz}^{\pm}$, given by the expressions

$$\tilde{h}_{xx}^{\pm} = -\frac{\hbar^2}{2\bar{m}}\bar{\nabla}_{\pm,xx}^2 + \left(\frac{\bar{m}\omega_0^2}{2} \pm \frac{\alpha}{R^3}\right)\tilde{\mu}_{\pm,xx}^2, \tag{27a}$$

$$\tilde{h}_{zz}^{\pm} = -\frac{\hbar^2}{2\bar{m}}\bar{\nabla}_{\pm,zz}^2 + \left(\frac{\bar{m}\omega_0^2}{2} \mp \frac{2\alpha}{R^3}\right)\tilde{\mu}_{\pm,zz}^2. \tag{27b}$$

The ground-state energy of two interacting dipoles $\tilde{E}_0$ is[2]

$$E_0 = \frac{\hbar\omega_0}{2}\left(2\sqrt{1 \pm \frac{\alpha}{R^3}} + \sqrt{1 \mp \frac{2\alpha}{R^3}}\right). \tag{28}$$

In order to calculate the net interaction energy between the two atoms V, we need to subtract the ground-state energy of two noninteracting dipoles, i.e., $V = \tilde{E}_0 - E_0$. Taylor expansion of the square root with respect to a small parameter ($\sqrt{1+\epsilon} \approx 1 + \epsilon/2 - \epsilon^2/8$) yields[2]

$$V \approx -\frac{3\alpha^2}{4R^6}. \tag{29}$$

It is now instructive to analyze the ground-state wave function Ψ for two interacting dipoles. With the definition of $\omega_{xx}^{+} = \omega\sqrt{1 + \alpha/R^3}$, the wave function associated with the coordinate $\tilde{\mu}_{xx}^{+}$ is given by

$$\tilde{\phi}_{xx}^{+} = \left(\frac{\bar{m}\omega_{xx}^{+}}{\pi\hbar}\right)^{1/4} \exp\left[-\frac{\bar{m}\omega_{xx}^{+}\tilde{\mu}_{+,xx}^2}{2\hbar}\right], \tag{30a}$$

$$\approx \mathcal{M} \exp\left[-\frac{\bar{m}(\omega + \Delta\omega_{xx}^{+})\tilde{\mu}_{+,xx}^2}{2\hbar}\right], \tag{30b}$$

where $\mathcal{M}$ is a normalization factor that does not depend on $\tilde{\mu}_{+,xx}^2$ and $\Delta\omega_{xx}^{+} = \alpha/R^3$. Similar definitions and statements can be made for the other eigencoordinates so that the two-dipole wave function can be written as

$$\Psi \propto \Psi_0 \exp\left[-\frac{\bar{m}\omega\alpha}{2\hbar R^3}\left(\pm(\tilde{\mu}_{xx}^{\pm})^2 \pm (\tilde{\mu}_{yy}^{\pm})^2 \mp 2(\tilde{\mu}_{zz}^{\pm})^2\right)\right]. \tag{31}$$

Applying the inverse transformation to that described in Eq. (25) yields

$$\Psi \propto \Psi_0 \exp\left[-\frac{v'}{2\hbar\omega_0}\right]. \tag{32}$$

The interesting aspect about this last equation is that to leading order. The exact wave function can be written as the product of the single-dipole wave function, Ψ_0, times a Jastrow factor $\exp[-v']$ (Ref. 11) for which v is simply given by $1/(2\hbar\omega_0)$.

2. Constructing higher-order trial wave functions in the dipole limit

For a given set of M pseudonuclei coordinates, it is possible to diagonalize the M-dipole Hamiltonian H_M,

$$H_M = \sum_{i=1}^{M} h_{0i} + \frac{1}{2}\sum_{i,j}^{M} v'(\mathbf{R}_{ij}), \tag{33}$$

numerically exactly within a time that scales with M^3. Of course, it would be desirable to have accurate estimates for the wave function in the ideal-dipole limit that can be obtained with more favorable scaling. Summing the dipole-dipole interaction over the system can be achieved as a linear operation in M (times log M) operations using fast Ewald

summation, for example, and hence Jastrow factors such as $\exp[-\gamma v']$ present no difficulties in DMC simulations.

The starting point of our treatment is to write the dipoles of all particles, which we assume to be identical for the sake of simplicity, into one vector μ with $3M$ components. This does not alter the form of the Hamiltonian H_M,

$$H_M = -\frac{\hbar^2}{2\bar{m}}\frac{\partial^2}{\partial \mu_\gamma^2} + \frac{1}{2}m\omega_0^2\mu_\gamma^2 - \frac{1}{2}\mu_\gamma T_{\gamma\beta}\mu_\beta, \tag{34}$$

where $T_{\gamma\beta}$ has become a symmetric $3M \times 3M$ matrix. As in Sec. II B 1, one can diagonalize T (in principle) with a unitary transformation S to $\tilde{T}_{\gamma\beta}=S_{\gamma\gamma}T_{\gamma\delta}S_{\delta\beta}$. The eigenvectors are then $\tilde{\mu}_\gamma=S_{\gamma\beta}\mu_\beta$ because the transposed S is the inverse transformation matrix, i.e., $S_{\gamma\gamma}S_{\gamma\beta}=\delta_{\gamma\beta}$. All masses m and unperturbed frequencies ω_0 remain invariant under a transformation with S as long as all m and all ω_0 are all identical, respectively. If m and ω_0 were atom dependent, then it would be necessary to define effective dipoles $\bar{\mu}_i=\mu_i/\sqrt{\bar{m}}$, which would diagonalize the kinetic energy. Moreover, part of the on-site potential-energy interaction would have to be transferred to the T matrix such that all on-site Hamiltonians become identical. This would then make the Hamiltonian formally identical with that in Eq. (34) and the same diagonalization techniques as those outlined further below could be applied.

Because the Hamiltonian is now diagonal in its $3M$ degrees of freedom, it can be written as

$$H = \sum_i h_{0i} - \frac{1}{2}\sum_i \tilde{T}_i\tilde{\mu}_i^2 \tag{35a}$$

$$= \sum_{i=1}^{3M} -\frac{\hbar^2}{2\bar{m}}\bar{\nabla}_i^2 + \bar{m}\omega_0^2\mu_i^2 - T_i\mu_i^2, \tag{35b}$$

where we have changed to roman indices to indicate that the summation convention is no longer implied. The exact wave function can now be written as

$$\Psi = \frac{1}{\mathcal{M}}\prod_{i=1}^{M}\exp\left[-\frac{\bar{m}\sqrt{\omega_0^2 - \tilde{T}_i/\bar{m}}\,\tilde{\mu}_i^2}{2\hbar}\right], \tag{36}$$

where $\mathcal{M}$ is again a normalization factor. The argument of the exponential can be expanded into a Taylor series, e.g.,

$$\omega_i = \omega_0\left\{1 - \frac{\tilde{T}_i}{2\bar{m}\omega_0^2} + \frac{1}{8}\left(\frac{\tilde{T}_i}{\bar{m}\omega_0^2}\right)^2 + \ldots\right\}, \tag{37}$$

with $\omega_i=\omega_0\sqrt{1-\tilde{T}_i/\bar{m}\omega_0^2}$. Thus, the (negative) argument in the exponential can be approximated via

$$\frac{m\omega_0}{2\hbar}\left\{\delta_{\gamma\beta} - \frac{1}{2\bar{m}\omega_0^2}\tilde{T}_{\gamma\beta} + \frac{1}{8(\bar{m}\omega_0^2)^2}\tilde{T}_{\gamma\gamma}\tilde{T}_{\gamma\beta}\right\}\tilde{\mu}_\gamma\tilde{\mu}_\beta, \tag{38}$$

where we have reverted to the summation convention. ($\tilde{T}$ is yet a diagonal matrix.) Instead of evaluating Eq. (38) in the basis of the "eigendipoles," one may as well return to the original representation and thus replace the individual terms in Eq. (38) as follows:

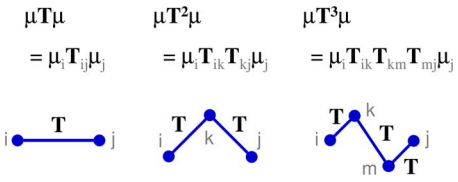

FIG. 1. (Color online) Diagrams representing the leading contributions in the exponent of the trial wave function [see Eq. (40)].

$$\delta_{\gamma\beta}\tilde{\mu}_\gamma\tilde{\mu}_\beta = S_{\gamma\gamma}S_{\gamma\beta}\tilde{\mu}_\gamma\tilde{\mu}_\beta = (\tilde{\mu}_\gamma S_{\gamma\gamma})(S_{\gamma\beta}\tilde{\mu}_\beta) = \mu_\gamma\mu_\gamma, \tag{39a}$$

$$\begin{aligned}\tilde{T}_{\gamma\beta}\tilde{\mu}_\gamma\tilde{\mu}_\beta &= \tilde{T}_{\gamma'\beta'}\delta_{\gamma\gamma'}\delta_{\beta\beta'}\tilde{\mu}_\gamma\tilde{\mu}_\beta \\ &= \tilde{T}_{\gamma'\beta'}S_{\gamma\gamma''}S_{\gamma'\gamma'}S_{\beta\beta''}S_{\beta''\beta'}\tilde{\mu}_\gamma\tilde{\mu}_\beta \\ &= S_{\gamma''\gamma'}\tilde{T}_{\gamma'\beta'}S_{\beta''\beta'}S_{\gamma\gamma''}\tilde{\mu}_\gamma S_{\beta\beta''}\tilde{\mu}_\beta = \tilde{T}_{\gamma''\beta''}\tilde{\mu}_{\gamma''}\tilde{\mu}_{\beta''},\end{aligned} \tag{39b}$$

and likewise

$$\tilde{T}_{\gamma\gamma}\tilde{T}_{\gamma\beta}\tilde{\mu}_\gamma\tilde{\mu}_\beta = T_{\gamma\gamma}T_{\gamma\beta}\mu_\gamma\mu_\beta. \tag{39c}$$

With this result, the trial wave function becomes

$$\Psi = \Psi_0\exp\left[\left\{\frac{-T_{\gamma\beta}}{2\bar{m}\omega_0^2} + \frac{T_{\gamma\gamma}T_{\gamma\beta}}{8(\bar{m}\omega_0^2)^2} + \ldots\right\}\mu_\gamma\mu_\beta\right]. \tag{40}$$

The different terms arising in Eq. (40) can be represented graphically as done in Fig. 1. The terms involving $\mu T^n\mu, n>1$ can be computed in order $(nM/2)\log M$ by iteratively evaluating $\mu_{\text{eff}}^{(k+1)}=T\mu_{\text{eff}}^{(k)}$, where $\mu_{\text{eff}}^{(1)}=\mu$, and then computing $\mu_{\text{eff}}^{(k)}\cdot\mu_{\text{eff}}^{(k)}$ using fast Ewald techniques.

Consistent with the calculation of the wave function, the net energy of the system E_0 is generated by summing over all frequencies of Eq. (37), specifically

$$E_0 = \frac{1}{2}\hbar\omega_0\sum_i\left\{1 - \frac{\tilde{T}_{ii}}{2\bar{m}\omega_0^2} + \frac{\tilde{T}_{i\beta}\tilde{T}_{\beta i}}{8(\bar{m}\omega_0^2)^2} + \ldots\right\} \tag{41a}$$

$$= \frac{1}{2}\hbar\omega_0\left\{\delta_{\gamma\gamma} - \frac{\tilde{T}_{\gamma\gamma}}{2\bar{m}\omega_0^2} + \frac{\tilde{T}_{\gamma\beta}\tilde{T}_{\beta\gamma}}{8(\bar{m}\omega_0^2)^2} + \ldots\right\} \tag{41b}$$

$$= \frac{1}{2}\hbar\omega_0\left\{3M - \frac{\mathbf{Tr}(T)}{2\bar{m}\omega_0^2} + \frac{\mathbf{Tr}(T^2)}{8(\bar{m}\omega_0^2)^2} + \ldots\right\}. \tag{41c}$$

Here, we have used the same notation as before, that is, the summation convention applies to Greek but not to Roman indices. The expansion can be seen as the diagrammatic expansion of Fig. 2 which because of Gaussian statistics contains only bubbles. The first correction term on the right hand side of Eq. (41) disappears because dipole tensor T is traceless in any representation. Each successive term in the energy expansion involves pair interactions, three-body interactions, four-body interactions, and so on.

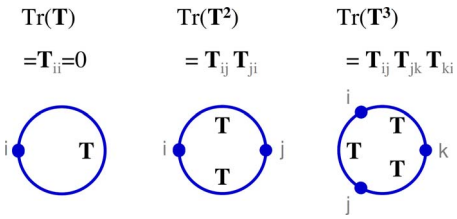

FIG. 2. (Color online) Diagrams representing the leading contributions to the dipole-dipole interaction energy as in Eq. (41c).

3. Summary of the QDO model in the dipole limit

In the above discussion, a useful hierarchy of trial function has been derived, the on site only, the on-site-plus-all-pair dipole, on-site-plus-all-pair-all-three-body dipole, and so on. Although the trial functions beyond the on-site-only are derived/presented in the dipole limit, it is simple matter to change variables back to the Cartesian representation of the full model and apply them to this more complex case. That is, the dipole limit is the first term in a multipole expansion of the full model and, thus, contributes an appreciable fraction of the total energy of the full QDO system.

4. Trial wave functions for the pair interaction limit of the full QDO model

Although the on-site-plus-all-pair dipole trial function has considerable content and is easy to implement for use in DMC simulations, higher-order-induced moment pair interactions are important for highly polarizable atoms such as xenon. It is therefore useful to develop a pair trial function for the full model, on-site-plus-all-pair-multipole trial function. We begin by writing an un-normalized Jastrow wavefunction ansatz for two Drude oscillators

$$\psi^{(2)} = \left[\prod_{i=1}^{2} \exp\left(-\frac{m\omega_0 \mathbf{r}_i^2}{2\hbar}\right)\right] \exp[-F_{dd}(\mathbf{r}_{12}+\mathbf{R}_{12}) - F_{dN}(\mathbf{r}_1+\mathbf{R}_{12}) - F_{dN}(\mathbf{r}_2-\mathbf{R}_{12})], \tag{42}$$

where $\mathbf{r}_i$ is the pseudoelectron displacement from its pseudonucleus $\mathbf{R}_i$ and $\mathbf{R}_{12}=\mathbf{R}_1-\mathbf{R}_2$ is the interpseudonuclear separation. Following earlier work which has suggested using the zero energy solution to Schrödinger's equation as Jastrow factors,[17,18] we write

$$\hat{H}\psi^{(2)} = 3\hbar\omega_0\psi^{(2)},$$

$$\hat{H} = \hat{T} + \frac{m\omega_0^2}{2}[\mathbf{r}_1^2+\mathbf{r}_2^2] + \frac{q^2}{|\mathbf{R}_{12}|} + \frac{q^2}{|\mathbf{r}_{12}+\mathbf{R}_{12}|} - \frac{q^2}{|\mathbf{r}_1+\mathbf{R}_{12}|} - \frac{q^2}{|\mathbf{r}_2+\mathbf{R}_{21}|}. \tag{43}$$

Keeping terms to first order in $\omega_0 F$ which is valid because F is small compared to ω_0 separates the problem into three identical equations of the form

$$(\hbar\omega_0)\mathbf{r}\cdot\nabla F = (\hbar\omega_0) r\frac{\partial F}{\partial r} = \frac{q^2}{|\mathbf{r}+\mathbf{R}|} - \frac{q^2}{|\mathbf{R}|}, \tag{44}$$

where $\mathbf{R}$ is assumed to line along the z axis. The solution is simply

$$F(\mathbf{r}+\mathbf{R}) = -\left(\frac{q^2}{\hbar\omega_0}\right)|\mathbf{R}|^{-1}\log[|\mathbf{R}|\cdot|\mathbf{R}+\mathbf{r}|+\mathbf{R}\cdot(\mathbf{R}+\mathbf{r})], \tag{45}$$

where we note that since

$$\nabla^2 F = 0, \tag{46}$$

the error is, in fact, of order $\mathcal{O}[(\hbar\omega_0)^0(\nabla F_\gamma\cdot\nabla F_\beta)] \sim \mathcal{O}[(\hbar\omega_0)^{-2}]$ and related to three-body correlations. Appropriate cutoff functions are introduced to avoid the singular behavior that arises when $|\mathbf{r}+\mathbf{R}|\approx 0$ similar to those introduced in the Coulomb potential itself as described above and in Refs. 9 and 10 (but not shown here to increase the clarity of the presentation).

5. Full QDO model for the simulation of xenon

The quantum Drude model for xenon employed herein is described in detail in Refs. 9 and 10. Briefly, in the gas-phase two-body limit, a short-range pair pseudonucleus-pseudonucleus repulsion is fit such that the QDO model reproduces the high-accuracy gas-phase BWLSL xenon-xenon pair potential of Ref. 23. The mass, charge, and frequency (m,q,ω_0) of the model were chosen to yield the dipole polarizability, α, the induced-dipole-induced-dipole dispersion coefficient, C_6, and the induced-dipole-induced-quadrupole +induced-quadrupole-induced-dipole dispersion coefficient, C_8, from Refs. 23 and 24. The parameters used to truncate the Coulomb interactions of the model were selected rather arbitrarily as the on site only trial function employed in Refs. 9 and 10 was not accurate enough to permit quantitative parameter fitting to the experimentally measured properties of the xenon crystal at $T=0$ (the results were of sufficient quality to obtain agreement to within $\approx 10\%$).

III. RESULTS

Here, the ability of the NC-DMC method and the trial wave functions developed for use with the QDO model to treat model and realistic systems is explored. The NC-DMC technique is validated through studies of the one-dimensional harmonic oscillator and then employed to study the realistic QDO model of xenon. The QDO trial wave functions are tested through NC-DMC and variational Monte Carlo (VMC) studies of the xenon dimer and the fcc-xenon crystal, where possible comparisons are made to analytical or experimental results as applicable. The notation M_{Xe} will be used to denote the number of xenon Drude oscillator atoms and N the number of NC-DMC walkers below. Diffusion Monte Carlo with rejection[20] appropriate for use with the more complex trial functions has not been implemented.

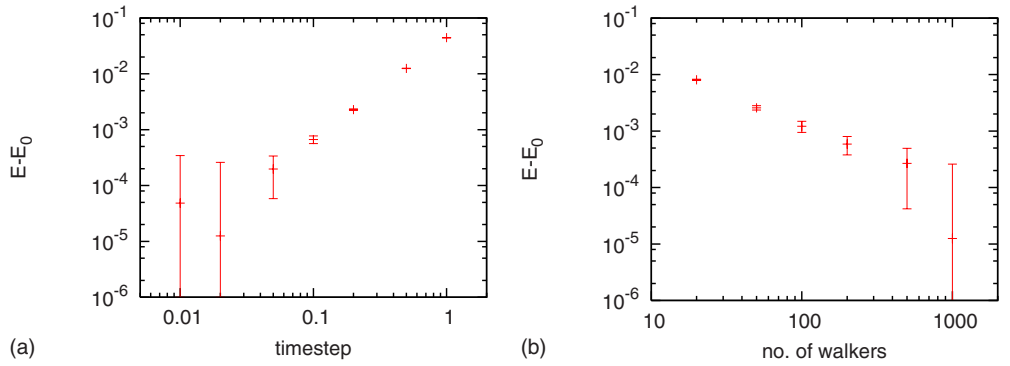

FIG. 3. (Color online) (a) The convergence of the ground-state energy with imaginary-time step for the one-dimensional harmonic oscillator computed using the NC-DMC method with $\psi_T=1$ and $N=1000$ walkers. (b) The corresponding convergence of the ground-state energy with walker number computed using an imaginary-time step of $\tau\hbar\omega=0.02$.

A. NC-DMC studies of the one-dimensional harmonic oscillator

In order to test the NC-DMC technique and the drift-diffusion evolution operator of the AppendixA 1, the harmonic oscillator is studied

$$\hat{H} = \hat{T} + \frac{m\omega^2\hat{x}^2}{2},$$

$$E_0 = \frac{\hbar\omega}{2},$$

$$\psi_0 = \left(\frac{m\omega}{\pi\hbar}\right)^{1/4} \exp\left(\frac{m\omega x^2}{2\hbar}\right),$$

$$\psi_T(\lambda) = \left(\frac{m\omega\lambda}{\pi\hbar}\right)^{1/4} \exp\left(\frac{m\omega\lambda x^2}{2\hbar}\right),$$

$$E_T = \langle\psi_T|\hat{H} - E_0|\psi_T\rangle = \frac{\hbar\omega(1-\lambda)^2}{4\lambda}. \quad (47)$$

Tests are performed using $\lambda=0$ and $\lambda=0.9$.

In Fig. 3, a NC-DMC study of the convergence of the ground-state energy with imaginary-time step, Fig. 3 (top), and walker number, Fig. 3 (bottom), is presented for the $\lambda=0$ trial function (no importance sampling). The results converge as τ^2 to the correct value [$E_0(\tau)-E_0$ is presented in the figure]. Approximately 200 walkers are required to generate converged results.

In Fig. 4, the same study is performed using the $\lambda=0.9$ trial function both with and without the improved drift-diffusion evolution operator. Again, appropriate convergence behavior is observed with the improved drift-diffusion evolution operator of Appendix A 1, exhibiting faster convergence with τ. Approximately 200 walkers seem to be required to generate accurate results.

B. Xenon dimer under the full QDO model

It is useful to evaluate the quality of the QDO trial functions presented in Sec. II through tests on the most basic system to which they can be applied, the xenon dimer. The variational dimer energy as a function of nuclear separation, $E_T(R)$, is given for all trial wave functions described in the text: the on site only trial function, the on-site-plus-dipole-dipole trial function, and the on-site-plus-all-pair-multipole model in Fig. 5. Results are compared to a high quality NC-DMC simulation estimate of $E_0(R)$ (the correct results). The on-site-plus-all-pair-multipole wave function performs particularly well, predicting the well depth to within 10%.

Next, the convergence of the ground-state energy of the xenon dimer at its minimum, $E_0(R_{\min})$, with imaginary-time step and walker number is presented for the on-site-plus-all-pair-multipole trial function under NC-DMC (see Fig. 6). The observed behavior is in accord with expectations (e.g., the convergence with N and τ is uniform and has the appropriate power-law dependence given the method of Ref. 20 has not been implemented).

C. Fcc-solid xenon under the dipole limit QDO model at $T=0$

Having demonstrated the stability and accuracy of the techniques on small systems, it is natural to examine larger systems for which high quality "exact" results can still be obtained. The dipole limit QDO model for the perfect fcc-xenon solid can be solved quasianalytically in reciprocal space (a $6n_{\text{site}}\times 6n_{\text{site}}$ matrix constructed by appropriate G-vector sums is diagonalized at each of the n_{cell}^3 k points in Brillouin zone where $n_{\text{site}}=4$ for the fcc lattice and n_{cell} is the number of fcc unit cells in the crystal of interest, as opposed to diagonalizing a single $3M_{\text{Xe}}\times 3M_{\text{Xe}}$ matrix). The results of a NC-DMC study of the dipole limit QDO model of the perfect fcc-xenon solid at the experimental lattice constant performed using $\hbar\tau=0.01$ $N=1000$ and the on-site-plus-dipole-dipole trial function are compared to the analytical results as a function of system size, M_{Xe}, in Fig. 7. Although the NC-DMC imaginary-time step must be decreased as $\sqrt{M_{\text{Xe}}}$ with increasing system size, the NC-DMC simulation estimates of the ground-state energies match the analytical answers within the error bars.

D. Fcc-solid xenon under the full QDO model at $T=0$

The results of Sec. III C suggest that the techniques are capable of generating high quality results for the nontrivial

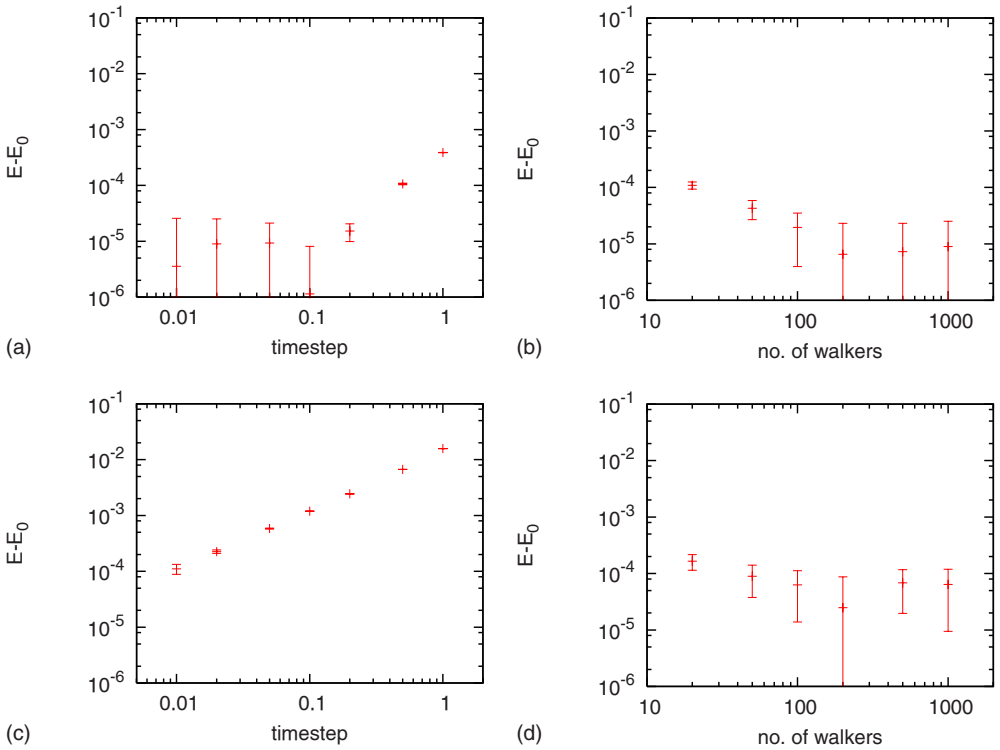

FIG. 4. (Color online) (a) The convergence of the ground-state energy with imaginary-time step for the one-dimensional harmonic oscillator computed using the NC-DMC method with $\psi_T=\psi_0(\lambda\omega);\lambda=0.9;\epsilon\neq 0$ and $N=1000$ walkers. (b) The corresponding convergence of the ground-state energy with walker number computed using an imaginary-time step of $\tau\hbar\omega=0.1$. (c) The convergence of the ground-state energy with imaginary-time step for the one-dimensional harmonic oscillator computed using the NC-DMC method with $\psi_T=\psi_0(\lambda\omega);\lambda=0.9;\epsilon=0$ and $N=1000$ walkers. (d) The corresponding convergence of the ground-state energy with walker number computed using an imaginary-time step of $\tau\hbar\omega=0.002$.

full QDO model of the fcc-xenon crystal where there are no analytical answers with which to compare. Proceeding carefully, therefore, in Fig. 8, the convergence of the ground-state energy with imaginary-time step for the full QDO model $M_{\mathrm{Xe}}=32$ atom xenon solid computed using the NC-DMC method with the on-site-plus-all-pair-multipole trial function and $N=1000$ walkers is given. Further computations on the QDO model solid given below were performed using $\hbar\tau=0.02$ a.u. and $N=1000$ and an appropriate reduction of τ as $\sqrt{M_{\mathrm{Xe}}}$ with increasing system size.

The ground-state energy of the fcc-xenon solid as a function of system size, M_{Xe}, at the experimentally determined lattice constant, $a_{\mathrm{eq}}=6.12$ Å, under the full model QDO is presented in Fig. 9 along with the extrapolation of the results to $M_{\mathrm{Xe}}\rightarrow\infty$ limit. The experimental $T=0$ binding energy is $E_0(a_{\mathrm{eq}})=-6.05$ mHartree/atom (Ref. 23) while the present full QDO predicts $E_0(a_{\mathrm{eq}})=-6.27$ mHartree/atom. The zero-point energy is estimated to be 0.2 mHartree/atom (Ref. 25) and hence the agreement is good. It is important to note that the full model QDO is fit to reproduce the BWLSL pair potential in the gas phase. The high-accuracy gas-phase pair potential predicts a $T=0$ crystal binding energy of $E_0(a_{\mathrm{eq}})=-6.81$ mHartree/atom. Thus, the full QDO model introduces substantial many-body corrections in the condensed phase.

In Fig. 10(a), the ground-state energy of the $M_{\mathrm{Xe}}=32$ atom fcc-xenon solid as a function of lattice constant, $E_0(a)$, is presented along with the variational energy, $E_T(a)$, of the on-site-plus-all-pair-multipole trial function. It is clear that $E_T(a)$ is not accurate enough to describe the solid well. Last, the ground-state energy of the $M_{\mathrm{Xe}}=32$ and $M_{\mathrm{Xe}}=256$ atom fcc-xenon solids as a function of lattice constant is presented in Fig. 10(b). The lattice constant predicted by the QDO model is in very good agreement with experiment ($a_{\mathrm{eq}}=6.12$ Å). In contrast, the BWLSL gas-phase pair potential, which is reproduced by the QDO model in the two-body gas-phase limit, predicts $a_{\mathrm{eq}}=6.04$ Å. Nuclear quantum effects (see the Appendix A 3) are estimated to increase the

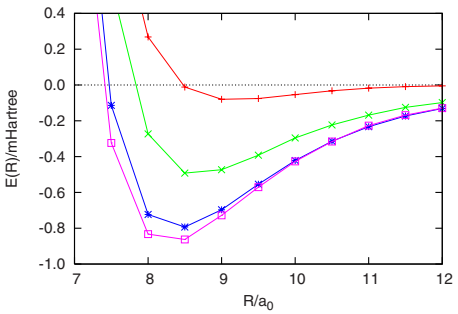

FIG. 5. (Color online) The variational energy as a function of nuclear separation $E_T(R)$ for the full QDO model xenon dimer is presented for all trial wave functions described in the text. (From top to bottom) The on-site-only trial function (plus sign), the on-site-plus-dipole-dipole trial function (x), and the on-site-plus-all-pair-multipole model (star). Results are compared to a converged NC-DMC study (box) of the dimer potential curve, $E_0(R)$.

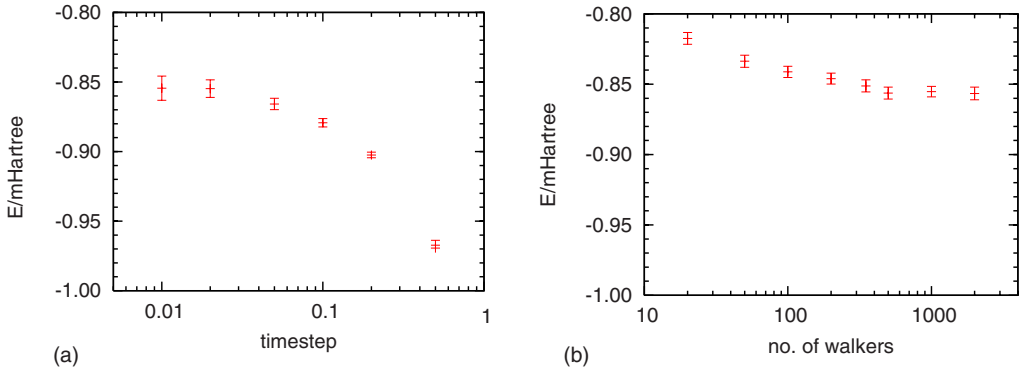

FIG. 6. (Color online) (a) The convergence of the ground-state energy with imaginary-time step for the full QDO model xenon dimer computed using the NC-DMC method with the on-site-plus-all-pair-multipole trial function. (b) The corresponding convergence of the ground-state energy with walker number computed using an imaginary-time step of $\hbar\tau=0.02$ a.u. The energy scale is on order 10 μHartree, stringently testing the method.

lattice constant by 0.03 Å. The QDO prediction of the bulk modulus for two system sizes, $\kappa=4.0\pm0.1$ GPa for $M_{\mathrm{Xe}}=32$ atoms and $\kappa=4.2\pm0.2$ GPa for $M_{\mathrm{Xe}}=256$ atoms, are in good agreement with each other and nuclear quantum effects are estimated to decrease these values by 0.3 GPa. Thus, the model prediction is within 3%–10% of the experimental value, $\kappa=3.64$ GPa. The BWLSL gas-phase pair potential predicts a rather large modulus, $\kappa=4.55$ GPa. Thus, the QDO does capture the many-body terms that arise in condensed phase reasonably well. These accurate simulation results show the present QDO xenon model is somewhat "stiff" in the solid phase although the lattice constant and the binding energy are predicted reasonably. In general, the QDO parameters need to be tuned to reflect the higher quality solid-state simulation data that can now be generated.

IV. SUMMARY AND CONCLUSIONS

In this paper, a NC-DMC technique is presented which strictly conserves the number of walkers along the stochastic trajectory without introducing weights. Corrections to the $\mathcal{O}(N^{-1})$ population bias were presented. The method, NC-DMC, is hence very stable and allows long runs to be performed in complex systems even when the trial function is not optimal and the imaginary-time step is taken to be large. The technique requires only a small modification of an existing DMC code and could potentially be applied to study a wide variety of problems. An improved propagator for the diffusion-drift evolution operator that can be generally implemented but is of particular interest for use with Gaussian trial functions where it is exact is also presented. The NC-DMC method was applied to study model and realistic systems and demonstrated to be stable and accurate.

The QDO is an elegant model that could be used to form the basis for next generation high-accuracy force fields as it naturally generates all long-range responses, in particular many-body polarization and dispersion. Using QDOs, the force-field designer need only concentrate on fitting short-range repulsive terms and cutoff functions designed to turn off the long-range interactions at close internuclear separations. If accurate single-point energies of the QDO model could be generated, these nontrivial QDO model parameters could be fit to experimental data and/or high-level quantum chemical computations of small systems, easily. Here, QDO trial functions for use with NC-DMC simulation studies per-

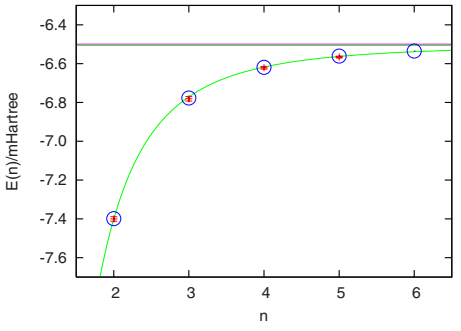

FIG. 7. (Color online) The convergence of the ground-state energy of the fcc-xenon solid at the equilibrium lattice constant as a function of system size ($n=n_{\mathrm{cell}}$) under the dipole limit QDO model computed using NC-DMC with the on-site-plus-dipole-dipole trial function, $N=1000$ walkers, and a time step of $\hbar\tau=0.01$. Simulation results (points) are compared to the analytical results (circles). A fit to the data is included $[f(n)=E_0-\Delta/n^3]$ along with the extrapolated value of $E_0=-6.5055$ mHartree/atom (top horizontal line), which is close to the large-N analytic result of $E_0=-6.4996$ mHartree/atom, calculated for $N=32\,000$ (slightly lower horizontal line).

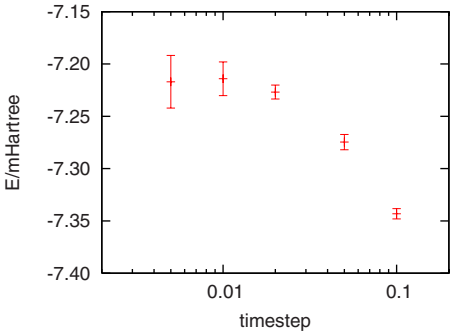

FIG. 8. (Color online) The convergence of the ground-state energy of the fcc-xenon solid as a function of imaginary-time step at the equilibrium lattice constant under the full QDO model computed using NC-DMC with the on-site-plus-all-pair-multipole trial function, with 32 atoms and $N=1000$ walkers.

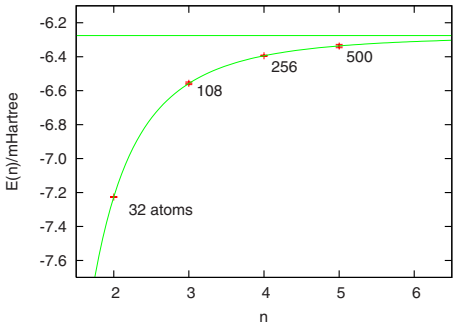

FIG. 9. (Color online) The convergence of the ground-state energy of the fcc-xenon solid as a function of system size ($n=n_{\mathrm{cell}}$) at the equilibrium lattice constant under the full QDO model computed using NC-DMC with the on-site-plus-all-pair-multipole trial function (the points), $N=1000$ walkers, and an imaginary-time step of $\hbar\tau=0.02$ a.u.. A fit to the data is included $[f(n)=E_0-\Delta/n^3]$ along with the extrapolated value of $E_0=-6.275$ mHartree/atom (top horizontal line).

formed to generate high-accuracy single-point ground-state energies are presented and then applied. It is found in studies of the fcc-xenon solid at $T=0$ that the trial functions presented herein are capable of generating high-accuracy ground-state energies for large system sizes when used in NC-DMC simulations. The proposed trial functions are of sufficiently high quality that the equilibrium lattice constant, the binding energy, and the bulk modulus of the QDO model fcc-xenon crystal at $T=0$ could be accurately determined. This represents a significant success. However, the present set of trial functions was not accurate enough to allow elastic constants to be predicted within the available computing budget. Current work involves employing correlated sampling techniques[26,27] and improved trial functions including three-body terms to generate more accurate results more efficiently.

ACKNOWLEDGMENTS

J.C. acknowledges support from Scottish Enterprise and the Edinburgh Parallel Computing Center. M.H.M. acknowledges support from NSERC and G.J.M. from IBM Research. A.J. and A.T. are supported by EPSRC-GB.

APPENDIX: DIFFUSION, DRIFT, BRANCHING, AND NUCLEAR QUANTUM EFFECTS

1. Diffusion and drift in DMC

As discussed in the text, a useful splitting of the non-Hermitian evolution operator given in Eq. (3) requires the application of $\exp[-\tau(\hat{T}+\hat{D})]$ to the distribution function, f. For arbitrary choice of ψ_T, the propagator cannot be obtained analytically. However, as we are interested in a small τ approximation to the operator, it is possible to make progress. First, basic $\exp[-\tau\hat{T}]$ evolution leads to the

$$f(x;\tau)=\left(\frac{m}{2\pi\hbar^2\tau}\right)^{1/2}\int dx'\,\exp\left[-\frac{m}{2\hbar^2\tau}(x-x')^2\right]f(x';0), \tag{A1}$$

where for simplicity we have restricted ourselves to one dimension and have assumed free space (open as opposed to periodic boundaries). As τ goes to zero, the Gaussian approaches a delta function thereby restricting the convolution to a small region of space about each point x. It is, therefore, possible to consider introducing the Taylor expansion for $d\log\psi_T/dx$ to first order which yields

$$\hat{D}f=\left(\frac{\hbar^2}{m}\right)\frac{d}{dx}\left[f(x)\left(\frac{d\log\psi_T(x')}{dx'}+(x-x')\frac{d^2\log\psi_T(x')}{dx'^2}\right)\right]. \tag{A2}$$

The expression is exact if ψ_T is Gaussian. The approximation leads to the evolution (which is again exact for Gaussian ψ_T) following[28]

$$f(x;\tau)=\int dx'\left(\frac{m}{2\pi\hbar^2\tau_{\mathrm{eff}}^{(1)}(x')}\right)^{1/2}\exp\left[-\frac{m}{2\hbar^2\tau_{\mathrm{eff}}^{(1)}(x')}\times\left(x-x'-\frac{\hbar^2\tau_{\mathrm{eff}}^{(2)}(x')}{m}\frac{d\log\psi_T(x')}{dx'}\right)^2\right]f(x';0), \tag{A3}$$

where

$$\tau_{\mathrm{eff}}^{(1)}(x)=\tau S[\tau\epsilon(x)],$$

$$\tau_{\mathrm{eff}}^{(2)}(x)=\tau S\left(\frac{\tau\epsilon(x)}{2}\right),$$

$$\epsilon(x)=\left(\frac{\hbar^2}{m}\right)\frac{d^2\log\psi_T(x)}{dx^2},$$

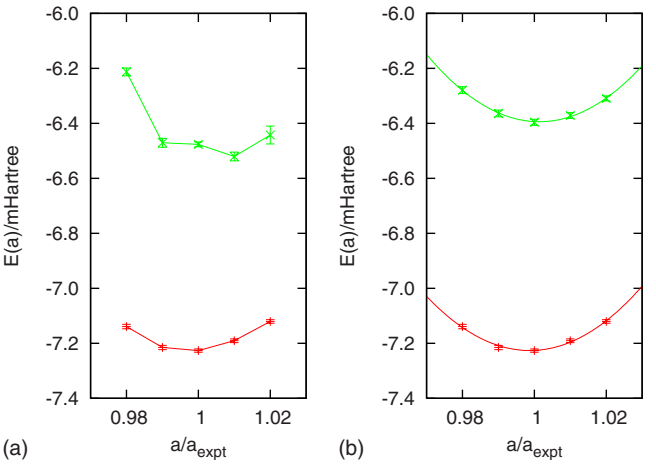

FIG. 10. (Color online) (a) The ground-state energy of the $M_{\mathrm{Xe}}=32$ atom fcc-xenon solid as a function of lattice constant $E_0(a)$ under the full QDO model computed using NC-DMC with the on-site-plus-all-pair-multipole trial function (bottom curve), $N=1000$ walkers, and an imaginary-time step of $\hbar\tau=0.02$ a.u. compared to the variational result of the on-site-plus-all-pair-multipole trial function (top curve). (b) The ground-state energy of fcc xenon for $M_{\mathrm{Xe}}=32$ atom (bottom curve) and $M_{\mathrm{Xe}}=256$ atom (top curve) cells solid as a function of lattice constant, $E_0(a)$, under the full QDO model computed using NC-DMC with the on-site-plus-all-pair-multipole trial function, $N=1000$ walkers, and an imaginary-time step of $\hbar\tau=0.02$ a.u.

$$S(\chi) = \exp(\chi)\frac{\sinh(\chi)}{\chi}, \tag{A4}$$

and the propagator is not symmetric because the drift-diffusion evolution operator is not Hermitian. The approximate evolution retains the norm-conserving property of the full operator

$$\int dx f(x;\tau) \equiv \int dx' f(x';0) \tag{A5}$$

and the $\tau_{\text{eff}}(x) \geq 0$ for all $\epsilon(x)$. (See Ref. 20 for a discussion of norm conservation in the presence of boundary-condition violations). If $\epsilon(x)$ is taken to be zero, $\tau_{\text{eff}}^{(1)} = \tau_{\text{eff}}^{(2)} = \tau$, then the commonly employed result is obtained.[17–19] To the best of our knowledge, Eq. (A3) has not appeared previously [e.g., in this form with nontrivial $\epsilon(x)$]. The formula is valid for periodic systems provided $\hbar^2\tau/(mL^2) \ll 1$, where L is the periodic box edge.

The above propagator can be applied to evolve a walker at position x' selected with probability $f(x';0)dx'$ to its new position x in the ensemble $f(x;\tau)$ by sampling a Gaussian random number $\zeta(x')$ with standard deviation given by $\sigma(x') = [\hbar^2\tau_{\text{eff}}^{(1)}(x')/m]^{1/2}$ and taking $x = x' + \zeta(x') + [\hbar^2\tau_{\text{eff}}^{(2)}(x')/m]d \log \psi_T(x')/dx'$. Appropriate cutoff functions can be introduced on $d \log \psi_T(x')/dx'$ (Ref. 20) and on $\epsilon(x')$ if necessary.

In multidimensional systems, the proposed evolution requires the computation of the second derivative matrix $\nabla\nabla \log(\psi_T)$ along with a rotation to a frame in which the matrix is diagonal. However, given that the DMC method already requires the computation of $\nabla^2 \log(\psi_T)$, it is a reasonable approximation to take the second derivative matrix to be diagonal (or take an isotropic average, $(1/d)\Sigma_\gamma \nabla_{i\gamma}^2 \log(\psi_T)$, for each particle i in d spatial dimensions to avoid inducing a bias through a particular choice of Cartesian coordinate system orientation). This simple approach is already an improvement on the usual approximation $\nabla\nabla \log(\psi_T) \approx 0$. For the QDO, specifically, the on-site term in ψ_T is both Gaussian in form: constant and dominant. It is, therefore, simple and straightforward to include a non-zero $\epsilon(x)$ in the diffusion-drift step. At present, we have only included the constant on-site term in our computations because we have observed that once this contribution to $\epsilon(x)$ is introduced, the imaginary-time step in the DMC studies is limited by the commutator between the branch and diffuse-drift evolution operators. However, improvements to the drift-diffusion propagator following the derivation given in Sec. II B 2 are possible and/or the drift-diffusion propagator can be applied in a multiple-time step fashion (n applications of the drift-diffusion propagator with time imaginary step, $\hbar\tau/2n$, before applying the branch operator with imaginary-time step, $\hbar\tau$).

It is useful to consider that performing a DMC simulation without branching is equivalent to sampling ψ_T^2 provided that the propagator is boundary condition satisfying and τ is taken sufficiently small because although $\exp[-\tau(\hat{T}+\hat{D})]$ preserves ψ_T^2 [e.g. $H \to H_T$ such that $E_0 \to (H_T\psi_T)/\psi_T$], approximations are made in its application. Since it is possible to sample ψ_T^2 using standard Metropolis Monte Carlo procedures, the efficacy of the approximations made in applying the drift-diffusion evolution operator can be investigated by performing an imaginary-time step convergence study of DMC sans branching (the walker number dependence of the DMC results is induced by the branch step only). In this way, measures can be taken to ensure that the imaginary-time step of the full DMC computations is limited only by the commutator between the branch and diffusion-drift terms. Additionally as described in Ref. 20, the errors in the drift-diffusion propagator can be reduced using a Metropolis Monte Carlo rejection sampling algorithm that imposes detailed balance by employing the approximate propagator as the *a priori* transition probability and ψ_T^2 as the limiting distribution. This approach has not been implemented herein but it can be employed with the improved drift-diffusion operator above without loss of generality. A minor drawback of Ref. 20 is that persistent or trapped configurations can occur (e.g., diffusion-drift moves of trapped configurations are accepted with very low weight) which requires careful attention to details in the method's implementation.

In Fig. 11(a), the results of an imaginary-time step study for the one-dimensional (1D) oscillator model presented in

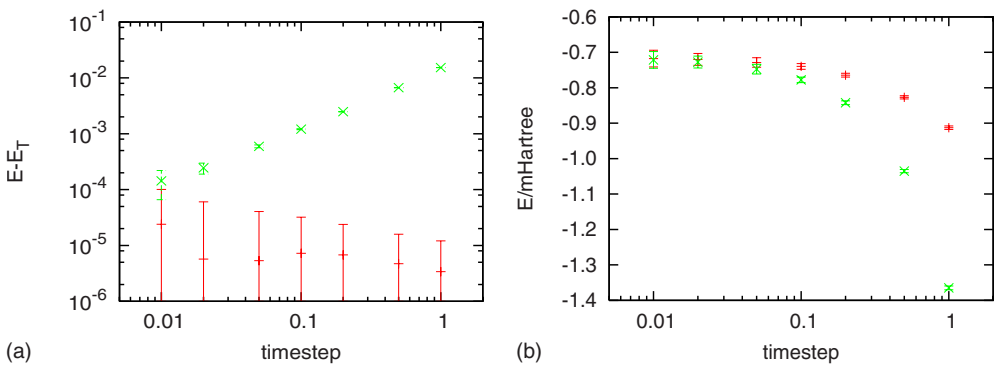

FIG. 11. (Color online) (a) The convergence of the variational energy with imaginary-time step both with and without the exact drift ($\epsilon \neq 0$: dash and $\epsilon \equiv 0$: cross), for the one-dimensional harmonic oscillator computed using the DMC method without branching and $\psi_T = \psi_0(\lambda\omega); \lambda = 0.9$. (b) The convergence of the variational energy with imaginary-time step both with and without the exact drift ($\epsilon \neq 0$: dash and $\epsilon \equiv 0$: cross) for the full QDO xenon dimer computing using the DMC method without branching and the on-site-plus-all-pair-multipole trial function.

Sec. III A under DMC with the branching step turned off are given. When $\epsilon(x)$ is taken to be nonzero, the computations yield correct results ($\langle\psi_T|(H-E_0)|\psi_T\rangle = \hbar\omega(1-\lambda)^2/(4\lambda) = E_T$) independent of imaginary-time step as is to be expected for a Gaussian model. With $\epsilon(x) \equiv 0$, the computations converge linearly with imaginary-time step to the correct result. In Fig. 11(b), a similar imaginary-time step study is presented for the QDO xenon dimer with ϵ taken to be zero and taken equal to the on-site interaction value. Again, taking $\epsilon \neq 0$ increases significantly the imaginary-time step at which convergence is obtained. However, both choices of ϵ converge to the result obtained from a standard Metropolis sampling study.

In order to demonstrate the utility of the local harmonic drift-diffusion propagator for systems in which the trial function is not predominantly Gaussian in character, we show the results for the hydrogen atom [$\psi_T = \exp(-r/a_0)$] within the isotropic diagonal second derivative approximation [$\epsilon = -2\tau\hbar^2/(3mra_0)$] simulated in Cartesian coordinates, in Fig. 12.

Finally, exact results for harmonic systems can be obtained and used to aid in accessing the accuracy of the new approach. The general expression

$$\langle x|\exp(-\tau\hat{O})|x'\rangle \equiv \langle x|\psi_T \exp(-\tau\hat{H})\psi_T^{-1}|x'\rangle \tag{A6}$$

can be evaluated analytically for the special case $H = T + m\omega^2 x^2/2$ and $H_T = T + m\omega^2\lambda^2 x^2/2$ as described in Ref. 28

$$\langle x|\exp(-\tau\hat{O})|x'\rangle = \left[\frac{m\omega}{2\hbar\,\sinh(\tau\hbar\omega)}\right]^{1/2} \times \exp\left\{-\frac{m\omega}{2\hbar}\left[\frac{1}{\sinh(\tau\hbar\omega)}(x-x')^2 + \tanh\left(\frac{\tau\hbar\omega}{2}\right)(x^2+x'^2) + \lambda(x^2-x'^2)\right]\right\}. \tag{A7}$$

The approximate propagator of the text can also be generated analytically for harmonic systems

$$\langle x|\exp(-\tau\hat{\tilde{O}}(\tau))|x'\rangle = \langle x|e^{-\tau\hat{o}_1/2}e^{-\tau\hat{o}_2}e^{-\tau\hat{o}_1/2}|x'\rangle = \left[\frac{m\omega a(\tau,\omega,\lambda)}{2}\right]^{1/2} \times \exp\left\{-\frac{m\omega}{2\hbar}[a(\tau,\omega,\lambda)(x-x')^2 + b(\tau,\omega,\lambda)(x^2+x'^2) + \lambda(x^2-x'^2)]\right\}, \tag{A8}$$

where

$$a(\tau,\omega,\lambda) = \left[\frac{\lambda}{\sinh(\tau\hbar\omega\lambda)}\right] \times \left[1 + \left(\frac{\tau\hbar\omega(1-\lambda^2)}{2\lambda}\right)\tanh\left(\frac{\tau\hbar\omega\lambda}{2}\right)\right]^{-1},$$

$$b(\tau,\omega,\lambda) = \lambda\,\tanh\left(\frac{\tau\hbar\omega\lambda}{2}\right) - 2a(\tau,\omega,\lambda) + \frac{2\lambda}{\sinh(\tau\hbar\omega\lambda)}. \tag{A9}$$

Since the approximate expression has the same form as the exact result, the finite τ propagator can be mapped onto its exact solution at arbitrary $\beta = P\tau$ through the definition of three effective parameters

$$\tilde{\omega}(\tau) = \left(\frac{2}{\tau\hbar}\right)\sinh^{-1}\left(\left[\frac{a(\tau,\omega,\lambda)}{2b(\tau,\omega,\lambda)}\right]^{1/2}\right),$$

$$\tilde{m}(\tau) = \left[\frac{m\omega a(\tau,\omega,\lambda,m)}{\tilde{\omega}(\tau)}\right]\sinh[\tau\hbar\tilde{\omega}(\tau)],$$

$$\tilde{\lambda}(\tau) = \left(\frac{m\omega\lambda}{\tilde{m}(\tau)\tilde{\omega}(\tau)}\right). \tag{A10}$$

Here, only the τ dependence of the effective parameters is referenced explicitly. Finite imaginary-time-step-dependent expressions for the DMC energy estimators discussed in AppendixA 2 follow

$$\tilde{E}_0(\tau) = \frac{\hbar\tilde{\omega}(\tau)}{2},$$

$$\tilde{E}_H(\tau) = \left\langle\frac{\hat{H}\psi_T(\lambda)}{\psi_T(\lambda)}\right\rangle_{\tilde{f}(\tau)} = \frac{\hbar\omega\lambda}{2} + \left\langle\frac{m\omega^2(1-\lambda^2)}{2}x^2\right\rangle_{\tilde{f}(\tau)} = \frac{\hbar\omega}{2}\left[\lambda + \left(\frac{[1-\lambda^2]\tilde{\lambda}(\tau)}{[1+\tilde{\lambda}(\tau)]\lambda}\right)\right], \tag{A11}$$

where

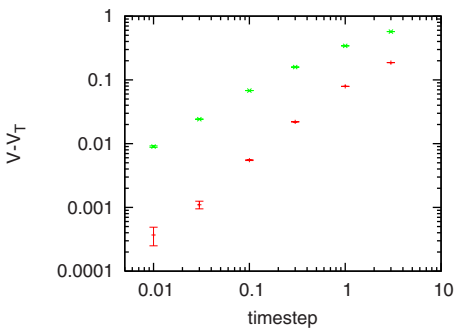

FIG. 12. (Color online) The convergence of $V_T = -\langle e^2/r\rangle_{\psi_T^2} = (-e^2/a_0)$ for the hydrogen atom, $\psi_T = \exp(-r/a_0)$, with imaginary-time step both with and without the isotropic diagonal approximation to the trial function second derivative matrix ($\epsilon = -2\hbar^2/(3mra_0)$: dash and $\epsilon \equiv 0$: cross) computed using the DMC method without branching in Cartesian coordinates.

$$\tilde{f}(x;\tau) = \left(\frac{\tilde{m}(\tau)\tilde{\omega}(\tau)[1+\tilde{\lambda}(\tau)]}{2\pi}\right)^{1/2} \times \exp\left(-\frac{\tilde{m}(\tau)\tilde{\omega}(\tau)[1+\tilde{\lambda}(\tau)]}{2}x^2\right). \quad \text{(A12)}$$

The $\tilde{E}_0(\tau)$ estimator exists when $\lambda \to 0$ because the limits of $a(\tau,\omega,0)=1/\tau\hbar\omega$ and $b(\tau,\omega,0)=\tau\hbar\omega/2$ are well defined. In the limit $\lambda \to 1$ both estimators properly yield the ground-state energy $E_0=\hbar\omega/2$.

In Fig. 13(a), the convergence of the NC-DMC method to the exact finite imaginary-time step results is shown for both a small and a large imaginary-time step. The convergence of the mean-field correction to NC-DMC is compared to straightforward NC-DMC at finite τ in Fig. 13(b). The correction allows about a factor of four reduction in the number of walkers required to achieve a given accuracy. In general, NC-DMC allows very high-accuracy results to be obtained straightforwardly.

2. Branching and estimating the energy in NC-DMC

The NC-DMC branching operator for each walker

$$\langle \vec{\mathbf{r}}|\exp[-\tau\hat{o}_2]|\vec{\mathbf{r}}\rangle = \{w^{(+)}(\vec{\mathbf{r}})n^{(+)}(\mathbf{r}_i) - \mathrm{Min}[w^{(-)}(\vec{\mathbf{r}})n^{(-)}(\mathbf{r}_i),1]+1\} \quad \text{(A13)}$$

can easily be applied to an ensemble of random walkers following earlier work.[16–20] First, one computes $n^{(\pm)}(\mathbf{r}_i)$, $\bar{n}^{(\pm)}(\vec{\mathbf{r}})$, and $w^{(\pm)}(\vec{\mathbf{r}})$ from the ensemble. Second, for each walker, $c_i=\mathrm{int}[w^{(+)}(\vec{\mathbf{r}})n^{(+)}(\mathbf{r}_i)]+1$ copies are included in the new ensemble plus one more if $\mathrm{frac}(w^{(+)}(\vec{\mathbf{r}})n^{(+)}(\mathbf{r}_i))$ is greater than a uniform random number. Here, the function int(a) indicates the integer part of the real number a and the function frac(a) indicates the fractional part of a [e.g., if $a=3.6$, then int$(a)=3$ and frac$(a)=0.6$]. Third, for each walker, one copy is removed from the ensemble if $\mathrm{frac}[w^{(-)}(\vec{\mathbf{r}})n^{(-)}(\mathbf{r}_i)]$ is greater than a uniform random number. Although the flux into/out of the ensemble have been forced to match, the random selection process may result in $N_{\mathrm{new}} \neq N$. However, having chosen new ensemble members with correct probability, all members of the new ensemble possess the same weight, $1/N_{\mathrm{new}}$. Therefore, it is correct and consistent to remove/add copies of randomly selected walkers in the new ensemble until $N_{\mathrm{new}}=N$ (e.g., walkers are copied with probability $1-N_{\mathrm{new}}/N; N_{\mathrm{new}}<N$ or deleted with probability $1-N/N_{\mathrm{new}}; N_{\mathrm{new}}>N$). In the absence of a flux-matching acceptance rule, the pruning procedure, $N_{\mathrm{new}} \to N$ would introduce bias as N would be required to fluctuate.

The ground-state energy can be estimated in two ways from a DMC simulation.[17–19] First, using the properties of a Hermitian operator

$$\int d\mathbf{r} f(\mathbf{r}) \frac{\hat{H}\psi_T(\mathbf{r})}{\psi_T(\mathbf{r})} = \int d\mathbf{r}\psi_T(\mathbf{r})\hat{H}\psi_0(\mathbf{r}) = E_0. \quad \text{(A14)}$$

Hence, an estimator for E_0 is simply

$$E_0^{(\mathrm{est},H)}(\vec{\mathbf{r}};\tau) = \frac{1}{N}\sum_i \frac{\hat{H}\psi_T(\mathbf{r}_i)}{\psi_T(\mathbf{r}_i)}, \quad \text{(A15)}$$

which is then averaged over the stochastic DMC process or DMC "trajectory" to yield an estimate for $\tilde{E}_0(\tau)$ [it has been assumed that the steady state is of the form $f(\tau)=\psi_T\psi_0(\tau)$]. The second estimator is constructed using the fact that $\langle \bar{n}^{(-)} - \bar{n}^{(+)}\rangle = 0$ should be zero if $\bar{E}=\tilde{E}_0(\tau)$ and $N \to \infty$ as described in the text

$$E_0^{(\mathrm{est},\tau)}(\vec{\mathbf{r}};\tau) = \bar{E} + \frac{\bar{n}^{(-)}(\vec{\mathbf{r}}) - \bar{n}^{(+)}(\vec{\mathbf{r}})}{\tau}. \quad \text{(A16)}$$

Typically, $\langle E_0^{(\mathrm{est},H)}\rangle$ has lower variance but if $\langle E_0^{(\mathrm{est},H)}\rangle$ does not closely agree with $\langle E_0^{(\mathrm{est},\tau)}\rangle$, the simulation should be rerun with a smaller time step $\hbar\tau$. As N increases $\langle E_0^{(\mathrm{est},\tau)}\rangle$ come into agreement with the $\bar{E}_{\mathrm{true}}$ of Eq. (15). If the ensemble average in Eq. (15) is not small, the computation should be rerun with an improved estimate of $\bar{E}$. The two

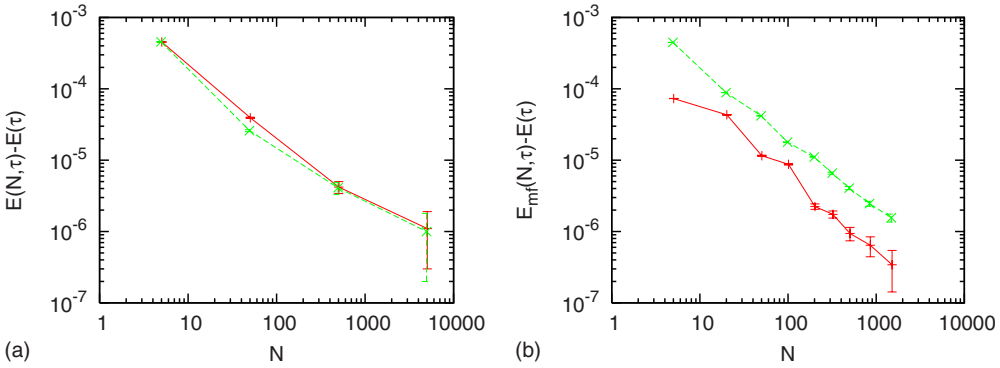

FIG. 13. (Color online) (a) The convergence of the ground-state energy as a function of walker number for the one-dimensional harmonic oscillator computed using the NC-DMC method with $\psi_T=\psi_0(\lambda\omega); \lambda=0.9; \epsilon\neq 0$ at two imaginary-time steps: $\tau\hbar\omega=0.6$ (dash) and $\tau\hbar\omega=0.06$ (cross). Convergence is presented relative the exact finite imaginary-time step results $\tilde{E}_H(0.6/\hbar\omega)-\hbar\omega/2=1.576\hbar\times 10^{-4}\hbar\omega$ and $\tilde{E}_H(0.06/\hbar\omega)-\hbar\omega/2=1.642\times 10^{-6}\hbar\omega$, respectively. (b) The improvement wrought by mean-field trajectory weighting procedure at imaginary-time step $\tau\hbar\omega=0.06$. The crosses are generated using the mean-field trajectory weighting correction while the x's are generated using NC-DMC.

above estimators, Eqs. (A15) and (A16) can be employed within the weighting technique(s) of the text to improve reduce the number of walkers required to reach a given accuracy.

It is important to select a good value of $\bar{E}$. A useful procedure is to start $\bar{E}$ equal to the variational energy, $E_v = \int d\mathbf{r}\psi_T(\mathbf{r})\hat{H}\psi_T(\mathbf{r})$, run NC-DMC for a few hundred steps, refine the quantities using Eq. (15), and so on until reasonable convergence is achieved. A long run may then be spawned with $\bar{E}$ fixed. The simulations are stable independent of $\bar{E}$ and the quality of a NC-DMC simulation can be assessed as described above. Again, the errors are absorbed into the corrections but decreasing the magnitude of the corrections increases the stability of the weighting procedure. Computing one-dimensional distribution such as $P(\bar{n}^{(+)})$, $P(\bar{n}^{(-)})$, and $P(\bar{n}^{(-)}-\bar{n}^{(+)})$ can also help judge the quality of the simulations. From the central limit theorem, as $N\rightarrow\infty$, $P(\bar{n}^{(\pm)})$ approaches a Gaussian characterized by mean $\sigma\sqrt{2/\pi}$ and standard deviation $\sigma\sqrt{(\pi-2)N_c/(\pi N)}$ and $P(\bar{n}^{(-)}-\bar{n}^{(+)})$ approaches a Gaussian characterized by zero mean and standard deviation $\sigma\sqrt{N_c/N}$, where N_c is a walker correlation number. If the quantity, $1-\exp[-\tau V_{\text{eff}}]$, itself exhibits zero mean Gaussian statistics with standard deviation, σ, then $N_c \equiv 1$.

The NC-DMC method divides walkers into two populations at every step, those below $\bar{E}$ and those above, and equalizes the flux out of the ensemble (arising from walkers with energy above $\bar{E}$) to the flux into the ensemble (arising walkers with energy below $\bar{E}$). Thus, the NC-DMC method can be become ill defined if all walkers have $V_{\text{eff}} \geq 0$ or $V_{\text{eff}} < 0$ for a given N-walker configuration. Making the reasonable assumption that the probability of any walker having a V_{eff} of sign positive/negative is 0.5 for the correct choice of $\bar{E}$, the probability that N walkers all have the V_{eff} with the same sign is $P^{(\text{all}\pm)}(N)=2^{1-N}$. For N as small as $N=50$, $P^{(\text{all}\pm)}(50)\approx 2\times 10^{-15}$, while for $N=20$, $P^{(\text{all}\pm)}(20)\approx 2\times 10^{-6}$. Thus, walker "sign collapse" is a rare event given large enough N. Due to walker correlations, the effective number of walkers is reduced, $N\rightarrow N/N_c$, where N_c is a walker correlation number. For sign-collapsed configurations, we can simply choose to take all present walkers into the next ensemble without prejudice (e.g., no flux in or out). This norm conversing choice is microscopically reversible because a sign collapse state is history independent (depends only on configuration). It effectively takes $\Pi_i f(\mathbf{r}_i)=\Pi_i \psi_T^2(\mathbf{r}_i)$ for any sign-collapsed configuration which is, in fact, exact for the case $\psi_T=\psi_0$ where $V_{\text{eff}}\equiv 0$, all configurations are sign collapsed (e.g., the sign of the number 0 is by convention positive) and there is no flux $\bar{n}^{(\pm)}\equiv 0$. The "accept all" choice for the sign-collapsed configurations defines the $N=1$ limit wherein NC-DMC samples $f(\mathbf{r})=\psi_T^2(\mathbf{r})$. It also preserves the variational character of the NC-DMC technique and leads to the "ensemble flux-matching" branch operator definition for each walker

$$\langle\vec{\mathbf{r}}|\exp[-\tau\hat{o}_2]|\vec{\mathbf{r}}\rangle = [\{w^{(+)}(\vec{\mathbf{r}})n^{(+)}(\mathbf{r}_i) - \text{Min}[w^{(-)}(\vec{\mathbf{r}})n^{(-)}(\mathbf{r}_i),1]\}\chi(\vec{\mathbf{r}})+1],$$

$$\chi(\vec{\mathbf{r}}) = 1-\left\{\prod_i \theta^{(-)}[V_{\text{eff}}(\mathbf{r}_i)]\right\}-\left\{\prod_i \theta^{(+)}[V_{\text{eff}}(\mathbf{r}_i)]\right\}, \tag{A17}$$

where $\chi(\vec{\mathbf{r}})=0$ for sign-collapsed configurations and $\chi(\vec{\mathbf{r}})=1$ otherwise. Similarly, configurations that are not sign collapsed but for which the self-consistent equation for $\bar{n}^{(-)}(\vec{\mathbf{r}})$, Eq. (10) would be required are also accepted without prejudice in the absence of boundary-condition violations. One may also "accept all" if $w^{(\pm)}\geq w^{(\text{cut})}\approx 100$.

Walker sign collapse occurs for a vanishingly small fraction of configurations given $N\geq 18$ and $\psi_T\neq\psi_0$. That is, sign-collapsed configurations become points of measure zero in the N-walker configuration space (e.g., $\vec{\mathbf{r}}$) for N remarkably small. The NC-DMC method is not recommended for use with $N<18$ where sign-collapsed configurations contribute more than one part in 1×10^5 unless ψ_T is a particularly good estimate of ψ_0. The "accept all" choice for sign-collapsed configurations ensures the method preserves the $\psi_T\rightarrow\psi_0; V_{\text{eff}}\rightarrow 0$ limit where $\bar{n}^{(\pm)}\equiv 0$ leads to ambiguities in the more naive NC-DMC acceptance rule and all configurations are, by definition, sign collapsed. For the case $\psi_T\neq\psi_0$, the accept all condition makes the variationally consistent choice $\Pi_i f(\mathbf{r}_i)=\Pi_i\psi_T^2(\mathbf{r}_i)$ for a set of configurations which rapidly approaches measure zero as $N\rightarrow\infty$. It, also, neatly defines the $N=1$ limit of the NC-DMC method to simply be a variational computation with trial function, ψ_T. If too many sign-collapsed configurations are identified, the number of walkers should be increased. Trajectory weighting either approximately in mean field or exactly, in principle, acts to correct for sign collapse (among other errors); for sign collapse $w^{(\pm)}(\vec{\mathbf{r}})\equiv 0$, which is easy to insert in the correction formalism. Again, the magnitude of the population bias vanishes as $\mathcal{O}(N^{-1})$, stabilizing the weighting procedure.

For completeness, we consider systems in which the diffusion-drift operator cannot be applied such that the boundary conditions are satisfied. The definitions of $\hat{o}_1$ and $\hat{o}_2$ of the main text should be reversed for this case. The QDO Hamiltonian studied herein is sufficiently simple that the drift-diffusion operator can be applied "properly." In general, any walker that violates the boundary conditions must be rejected and its rejection probability $n^{(-)}(\mathbf{r}_i)$ cannot be scaled so that it is different from unity. If $\bar{n}^{(-)}<\bar{n}^{(+)}$ and the self-consistency condition given in Eq. (10) has a solution, the NC-DMC method needs no modification. When $\bar{n}^{(-)}<\bar{n}^{(+)}$, the new self-consistency condition,

$$w^{(-)}(\vec{\mathbf{r}})\bar{n}^{(-)}(\vec{\mathbf{r}}) = \sum_i n^{(-)}(\mathbf{r}_i)\theta^{(+)}[n^{(-)}(\mathbf{r}_i)-1] + w^{(-)}(\vec{\mathbf{r}})\sum_i n^{(-)}(\mathbf{r}_i)\theta^{(-)}[1-n^{(-)}(\mathbf{r}_i)],$$

$$w^{(-)}(\vec{\mathbf{r}}) = \frac{w^{(-)}(\vec{\mathbf{r}})\bar{n}^{(-)}(\vec{\mathbf{r}})}{4w^{(-)}(\vec{\mathbf{r}})\bar{n}^{(-)}(\vec{\mathbf{r}})-2\bar{n}^{(+)}(\vec{\mathbf{r}})}>0, \tag{A18}$$

is imposed. For those rare N-walker configurations for which self-consistent solutions do not exist, all walkers that violate the boundary conditions are removed. The new ensemble of size $N_{\text{new}}<N$ is then grown back to size N by randomly

copying the remaining walkers with equal probability as described in the first paragraph of this section. Again, these fixes for configurations of measure zero are not history dependent. The method of Ref. 20 can be implemented so as to reject boundary condition violating moves at the drift/diffusion step thereby obviating the above procedure and permitting the definitions of $\hat{o}_1$ and $\hat{o}_2$ in the main text to be employed.

3. Nuclear quantum effects

The relative importance of quantum effects due to the nuclear motion of Lennard-Jones (LJ) atoms can be quantified with the de Boer parameter, $\Lambda = h/\sigma\sqrt{m\epsilon}$, where m is the mass of the LJ atom and σ and ϵ are its LJ interaction radius and energy, respectively.[29] Properties of Lennard-Jonesium in reduced units depend linearly on Λ, for example, its reduced density can be fitted to the equation $\rho^* = -1.0789\Lambda - 0.845\Lambda$, as ascertained from Table II in Ref. 30. Using results for solid argon on the quantum effects in the lattice constant and bulk modulus from the literature,[31] we can use this linear dependence on Λ to estimate the quantum effects in xenon. The LJ parameters for argon used in Ref. 31 were $\sigma = 3.405$ Å and $\epsilon = 120\ k_B K$, while reasonable values for the condensed phase of xenon are $\sigma = 4.055$ Å and $\epsilon = 228\ k_B K$, thus the ratio $\Lambda_{Xe}/\Lambda_{Ar} = 0.42$. The relative difference in lattice constant and elastic constants of quantum versus classical for argon were reported to be 1.2% and −17%, respectively. Given the ratio for Λ stated above, a 0.5% increase in the classical limit lattice constant of xenon and a 7% decrease in the classical limit bulk modulus of xenon due to quantum effects can be expected.

*martyna@us.ibm.com

[1] R. Eisenschitz and F. London, Z. Phys. **60**, 491 (1930).
[2] J. O. Hirschfelder, C. F. Curtiss, and R. B. Bird, *The Molecular Theory of Gases and Liquids* (Wiley, New York, 1964).
[3] J. Miyazaki, J. A. Barker, and G. M. Pound, J. Chem. Phys. **64**, 3364 (1976).
[4] J. A. Barker, Mol. Phys. **80**, 815 (1993).
[5] R. Zhou, X. Huang, C. J. Margulis, and B. J. Berne, Science **305**, 1605 (2004).
[6] B. M. Axilrod and E. Teller, J. Chem. Phys. **11**, 299 (1943).
[7] A. D. MacKerell, Jr., D. Bashford, M. Bellott, R. L. Dumbrack, J. D. Evanseck, M. J. Field, S. Fischer, H. Guo, S. Ha, D. Joseph-McCarthy, L. Kcuhnir, K. Kuczera, F. T. K. Lau, C. Mattos, S. Michnick, T. Ngo, D. T. Nguyen, B. Prodhom, W. E. Reiher III, B. Roux, M. Schlenkrich, J. C. Smith, R. Stote, J. Straub, M. Watanabe, J. Wiorkiewicz-Kuczera, D. Yin, and M. Karplus, J. Phys. Chem. B **102**, 3586 (1998).
[8] D. C. Langreth, M. Dion, H. Rydberg, E. Schroeder, P. Hyldgaard, and B. I. Lundqvist, Int. J. Quantum Chem. **101**, 599 (2005).
[9] T. W. Whitfield and G. J. Martyna, Chem. Phys. Lett. **424**, 409 (2006).
[10] T. W. Whitfield and G. J. Martyna, J. Chem. Phys. **126**, 074104 (2007).
[11] F. Brown and C. L. Gravel, Phys. Rev. **98**, 442 (1955).
[12] R. Assaraf, M. Caffarel, and A. Khelif, Phys. Rev. E **61**, 4566 (2000).
[13] M. Calandra Buonaura and S. Sorella, Phys. Rev. B **57**, 11446 (1998).
[14] J. H. Hetherington, Phys. Rev. A **30**, 2713 (1984).
[15] R. C. Grimm and R. G. Storer, J. Comput. Phys. **7**, 134 (1971).
[16] J. B. Anderson, J. Chem. Phys. **63**, 1499 (1975).
[17] Malvin H. Kalos and Paula A. Whitlock, *Monte Carlo Methods* (Wiley, New York, 1986).
[18] B. L. Hammond, W. A. Lester, Jr., and P. J. Reynolds, *Monte Carlo Methods in Ab Initio Quantum Chemistry* (World Scientific, London, 1994).
[19] D. M. Ceperley, Rev. Mod. Phys. **67**, 279 (1995).
[20] C. J. Umrigar, M. P. Nightingale, and K. J. Runge, J. Chem. Phys. **99**, 2865 (1993).
[21] R. M. Wilcox, J. Math. Phys. **8**, 962 (1967).
[22] M. P. Allen and D. J. Tildesley, *Computer Simulations of Liquids* (Claredon, Oxford, 1989).
[23] J. A. Barker, R. O. Watts, Jong K. Lee, T. P. Schafer, and Y. T. Lee, J. Chem. Phys. **61**, 3081 (1974).
[24] J. M. Standard and P. R. Certain, J. Chem. Phys. **83**, 3002 (1985).
[25] M. V. Bobetic and J. A. Barker, Phys. Rev. B **28**, 7317 (1983).
[26] M. H. Müser, P. Nielaba, and K. Binder, Phys. Rev. B **51**, 2723 (1995).
[27] C. Filippi and C. J. Umrigar, Phys. Rev. B **61**, R16291 (2000).
[28] R. P. Feynman, *Statistical Mechanics* (Benjamin, New York, 1972).
[29] J. de Boer, Physica (Amsterdam) **14**, 139 (1948).
[30] C. Chakravarty, J. Chem. Phys. **116**, 8938 (2002).
[31] P. Schöffel and M. H. Müser, Phys. Rev. B **63**, 224108 (2001).